Detection of metabolite-protein interactions in complex biological samples by high-resolution relaxometry: toward interactomics by NMR

Ziqing Wang, Simone Pisano, Veronica Ghini, Pavel Kadeřávek, Milan Zachrdla, Philippe Pelupessy, Morgan Kazmierczak, Thorsten Marquardsen, Jean-Max Tyburn, Guillaume Bouvignies, et al.

Detection of metabolite-protein interactions in complex biological samples by high-resolution relaxometry: toward interactomics by NMR

Ziqing Wang[1], Simone Pisano[1], Veronica Ghini[2], Pavel Kadeřávek[1,#], Milan Zachrdla[1,†], Philippe Pelupessy[1], Morgan Kazmierczak[1], Thorsten Marquardsen[3], Jean-Max Tyburn[4], Guillaume Bouvignies[1], Giacomo Parigi[2,5,6], Claudio Luchinat[2,5,6*], Fabien Ferrage[1,*]

1. Laboratoire des Biomolécules, LBM, Département de chimie, École normale supérieure, PSL University, Sorbonne Université, CNRS, 75005 Paris, France

2. Consorzio Interuniversitario Risonanze Magnetiche MetalloProteine (CIRMMP), via Sacconi 6, Sesto Fiorentino, 50019 Italy

3. Bruker BioSpin GmbH; Silberstreifen 4, 76287 Rheinstetten, Germany

4. Bruker BioSpin ; 34 rue de l'Industrie BP 10002, 67166 Wissembourg Cedex, France

5. Magnetic Resonance Center (CERM), University of Florence, via Sacconi 6, Sesto Fiorentino, 50019 Italy

6. Department of Chemistry "Ugo Schiff", University of Florence, via della Lastruccia 3, Sesto Fiorentino, 50019 Italy

Fabien Ferrage – Laboratoire des Biomolécules, LBM, Département de chimie, École normale supérieure, PSL University, Sorbonne Université, CNRS, 75005 Paris, France. Email: fabien.ferrage@ens.psl.eu

Claudio Luchinat – Magnetic Resonance Center (CERM) and Department of Chemistry "Ugo Schiff", University of Florence, and Consorzio Interuniversitario Risonanze Magnetiche MetalloProteine (CIRMMP), Sesto Fiorentino, Italy. Email: luchinat@cerm.unifi.it

ABSTRACT: Metabolomics, the systematic investigation of metabolites in biological fluids, cells or tissues, reveals essential information about metabolism and diseases. Metabolites have functional roles in myriads of biological processes, as substrates and products of enzymatic reactions, but also as cofactors and regulators of large numbers of biochemical mechanisms. These functions involve interactions of metabolites with macromolecules. Yet, methods to systematically investigate these interactions are hitherto still scarce. In particular, there is a need for techniques suited to identify and characterize weak metabolite-macromolecule interactions directly in complex media such as biological fluids. Here, we introduce a method to investigate weak interactions between metabolites and macromolecules in biological fluids. Our approach is based on high-resolution NMR relaxometry and does not require any invasive procedure or separation step. We show that we can detect interactions between small and large molecules in human blood serum and quantify the size of the complex. Our work opens the way for investigations of metabolite- (or other small molecules) protein interactions in biological fluids for interactomics or pharmaceutical applications.

INTRODUCTION

Biological fluids are complex mixtures of low-molecular weight molecules, i.e. metabolites, macromolecules, i.e. proteins and nucleic-acid fragments, and cells.[1-2] Metabolites, such as amino acids, lipids and carbohydrates, are intermediates or end products of metabolism. They constitute a unique chemical fingerprint of the metabolic status and represent valuable markers for various diseases. Metabolites also affect cellular activities by binding to macromolecules to carry out their functions in signaling, regulation and other cellular processes.

During the last twenty years, metabolomics[3-7] and proteomics[8-11] have been established as crucial analytical fields for the identification of metabolites and proteins, respectively, with a strong impact in biology and medical diagnostics.[11-14] NMR has proven to be a powerful tool for metabolomics.[15-32] On the other hand, the investigation of the interactions between all biological molecules in living organisms (i.e. metabolites, proteins, nucleic acids), called interactomics, has developed non uniformly.[33-34] The systematic determination of protein-protein interactions (PPIs) has been performed at the scale of full proteomes, including the human proteome,[35-40] and has proven to be an accelerator for drug discovery through systematic determination of host-pathogen protein-protein interactions.[41] On the other hand, the determination of metabolite-protein interactions (MPIs) is still under development.[42-43] MPIs are amongst the least studied in interactomics, mainly due to the lack of systematic analytical techniques. Analytical methods to probe MPIs have been reported, but most of them involve chemical modification of metabolites (e.g. by inserting radioactive or fluorescent handles) or proteins (with tagging or isotope labelling),[44-45] or tedious separation methods (electrophoresis, chromatography, ultrafiltration, etc.).[44, 46-47] Despite being fairly robust, these approaches can be time-consuming, they rely on complex protocols and none of them is performed in situ (i.e. within a biological tissue or liquid), which increases the risk of bias. Weak interactions between metabolites and macromolecules in biological fluids are particularly challenging to characterize with existing approaches and an analytical method designed to systematically identify interactions between metabolites and macromolecules, particularly weak MPIs, is in need.

Many NMR methods have been developed to investigate specific interactions between small and large molecules. They often rely on physical properties that are different in the small molecule and the complex. Several methods, based on the difference in dipolar cross-relaxation in small and large molecules are efficient at identifying interactions between a small molecule and a macromolecule, with little information on the macromolecule.[48-52] Diffusion-edited NMR experiments probe the effective size of small molecules.53 Effective transitional diffusion coefficients are weakly altered by low-affinity binding.[54-55] In addition, estimating the size of a complex from the apparent diffusion of a small molecule requires, at least, a titration experiment. By contrast, nuclear magnetic relaxation is probably the most sensitive property for assessing molecular dynamics and size. The magnetic-field dependence of relaxation rates identifies clearly rotational diffusion correlation times, which change dramatically depending on molecular size. By measuring relaxation rates over a broad range of magnetic fields (typically 100 µT to a few T), fast field-cycling (FFC) relaxometry[56] can determine overall diffusion correlation times of all the species in a sample.[57-60] However, FFC is a low-resolution technique, characterizing the collective relaxation of nuclei of the whole samples and it is not suitable for the identification of individual interactions in complex mixtures.

Here, we introduce high-resolution NMR relaxometry as a powerful analytical method to investigate MPIs in biological fluids. High-resolution relaxometry (HRR) combines the

analytical power of high-resolution NMR with relaxometry, exploiting the stray field of a commercial NMR magnet as variable field.[61-63] We demonstrate that weak interactions of metabolites with proteins can be identified from the field-dependence of proton relaxation rates of metabolites in human blood serum. We show that the size of the metabolite-protein complex could be determined for two small molecules and serum albumin, in a model sample as well as in human blood serum. Finally, we demonstrate that our approach can be used to characterize binding competition. Our work illustrates the potential of high-resolution relaxometry for the investigation of interactions of small molecules and proteins in complex media, in particular biological fluids, with potential applications in interactomics and drug screening.

HIGH-RESOLUTION RELAXOMETRY

The principle of relaxometry is to measure nuclear spin relaxation rates over several orders of magnitude of magnetic fields. In FFC, after polarization, an electro-magnet is switched to lower magnitude for relaxation and back to higher magnitude before detection. Another way of sampling a large span of magnetic fields is to physically move the sample away from the center of the coil of a high-resolution NMR magnet.[62-70] The latter approach allows one to couple high-resolution NMR detection with relaxometry. For example, phosphorus-31 high-resolution relaxometry has been used to probe the binding of a small molecule to a protein *in vitro*.[69-70] Here, we discuss how proton high-resolution relaxometry can be used as a ubiquitous probe of metabolite interactions in biological fluids. The rotational diffusion correlation time (τ_c) is proportional to the volume of a molecule, thus it changes dramatically when a small molecule binds to a macromolecule. In solution, unbound metabolites have small τ_c of about tens to hundreds of picoseconds, whereas macromolecule-bound metabolites have τ_c from a few nanoseconds to about a microsecond.[58, 71] If the exchange between the

free and bound form of the metabolite is fast with respect to relaxation rates, $k_{ex} \gg |R_1B - R_1F|$ the measured effective longitudinal relaxation rate R_1^{eff} can be written as the weighted average between the longitudinal relaxation rates of the free form R_1^F and that of the bound form R_1^B:

$$R_1^{eff} = p_F R_1^F + p_B R_1^B \qquad (1)$$

where p_F and p_B are the populations of the free and bound states of the small molecule ($p_F + p_B = 1$).

Here, we present a simple model for the relaxation of methyl group protons in a small molecule binding transiently to a macromolecule. In the free form, we only consider the dipolar interactions between identical protons inside the methyl group:

$$R_1^F = A_{methyl}[J(\omega_H, \tau_c^F) + 4J(2\omega_H, \tau_c^F)] \qquad (2)$$

where the effective dipolar constant is $A_{methyl} = S^2 \frac{3}{32} \frac{\mu_0^2 \gamma_H^4 \hbar^2}{\pi^2 r_{HH}^6}$, S^2 is the order parameter for intra-methyl dipole-dipole interactions, μ_0 is the permeability of vacuum, γ_H is the gyromagnetic ratio of the proton and r_{HH} is the distance between two protons inside the methyl group (as found in Ref. 72) The spectral density function $J(\omega, \tau_c)$ is the Fourier transform of the correlation function for nuclear spin interactions, where $\omega_H = -\gamma_H B_0$ is the Larmor frequency of the considered proton, B_0 is the magnetic field, and τ_c^F is the rotational correlation times of the small molecule free in solution. Assuming infinitely fast rotation of the methyl group, the dipolar constant is simply scaled by the order parameter $S^2 = 1/4$. In the bound form, we consider that relaxation is dominated by dipole-dipole interactions between methyl-group protons and surrounding protons of the environment, including intramolecular and intermolecular contributions:

$$R_1^B = A_B[J(0, \tau_c^B) + 3J(\omega_H, \tau_c^B) + 6J(2\omega_H, \tau_c^B)] \qquad (3)$$

The dipolar constant is $A_B = S^2 \frac{1}{64} \frac{\mu_0^2 \gamma_H^4 \hbar^2}{\pi^2 r_{env}^6}$, where r_{env} is the distance between the methyl group protons and a single effective proton representing all other protons in the complex, and τ_c^B is the rotational correlation times of the small molecule when it is bound to a macromolecule (*i.e.* the correlation time of the macromolecule). We introduce the additional hypothesis that the population of the bound form is much smaller than the population of the free form: $p_B \ll p_F$ and $p_F \approx 1$. Under these hypotheses, the number of free parameters in the model is reduced to three: the correlation times τ_c^F and τ_c^B and the product $p_B A_B$. These hypotheses have been tested in the analyses of high-resolution relaxometry profiles of a model compound (see below and SI, section 3).

Here, we use the following simple expression for the spectral density function $J(\omega, \tau_c)$ to model the overall rotational diffusion in the case of isotropic motion:

$$J(\omega, \tau_c) = \frac{2}{5} \frac{\tau_c}{1+\omega^2 \tau_c^2}. \qquad (4)$$

NMR relaxation dispersion (NMRD) profiles, obtained through a broad range of magnetic fields, allow one to map the spectral density function over a wide range of frequencies and, hence, determine correlation times. As noted in the expressions for $J(\omega, \tau_c)$, when the correlation time is small (free state of a small molecule), we have $\omega\tau_c \ll 1$ over the entire range of magnetic fields. This is the so-called extreme narrowing regime, where longitudinal relaxation rates due to dipole-dipole interactions are small and mostly independent of the magnetic field. For macromolecules, a strong dispersion is expected over the range of magnetic fields where $\omega\tau_c \sim 1$. The low-field limit of longitudinal relaxation rates is proportional to the correlation time τ_c, making NMRD profiles of macromolecules very sensitive to the molecular size. A dispersion at low magnetic fields ($B_0 < 1$ T) in the NMRD profile of a proton in a small molecule is a clear signature of transient binding to a macromolecule, (Fig. 1). Recording a full NMRD

profile provides enough information to determine unambiguously the correlation time for the small molecule in its bound state.
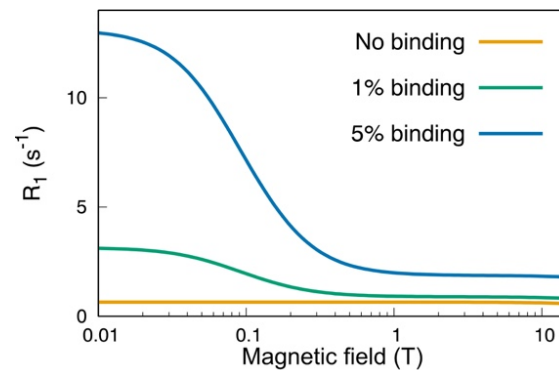

Figure 1. Illustration of the effect of binding of a small molecule (τ_c^F = 50 ps) to a macromolecule (τ_c^B = 25 ns) on the longitudinal relaxation dispersion profile of the small molecule. The yellow, green and blue curves show NMRD profiles of the small molecule with a bound fraction of 0%, 1% and 5%, respectively. The model presented in Equations 1-4 was used for the calculation and only the dipolar interaction with the effective protein protons is considered in the bound form. The effective dipolar interaction amplitude is set to 109 s^{-2}, corresponding to r_{env} = 229 pm.

High-resolution relaxometry provides relaxation rates for each individual signal in a high-resolution spectrum. Each nucleus will show a different relaxometry signature due to its specific tumbling correlation time and internal dynamics. When components of different sizes interact in a mixture, we expect a clear signature of this interaction in individual NMRD profiles (Fig. 1). An HRR experiment starts with polarization of nuclear spins at the high-field position (Fig. 2, 2). The sample is then transferred to a predefined position of the stray field of the magnet (Fig. 2, 3) for relaxation. Finally, the sample is sent back to the high-field position for detection. This setup allows one to benefit from both high-sensitivity and high-resolution provided by the homogeneous high magnetic field, and to collect relaxation rates across a broad range of magnetic fields (here, 15 mT to 14.1 T).
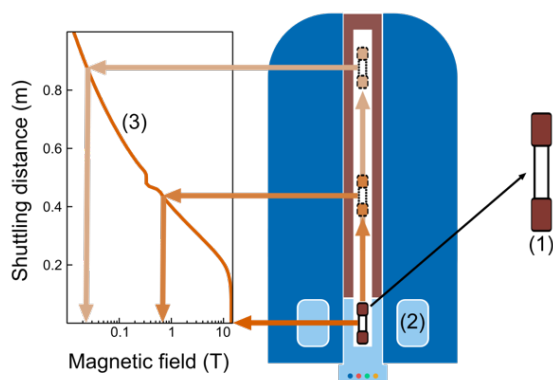
Figure 2. Schematic cross-section view of the high-resolution relaxometry system: (1) shuttle tube with an active volume of 60 µL and end caps (brown rectangles) protecting the tube during transfers and landing; (2) Magnet operating at 14.1 T (600 MHz) for polarization and detection, and triple-resonance shuttle probe with z-gradient; (3) Magnetic fields as function of the distance to the magnetic center. The plateau at 0.33 T is due to the presence of ferroshims in the bore of our magnet.[73] During an HRR experiment, the sample is transferred between the probe (sample shown in solid-line contours) and a preset position inside the magnet (sample shown as dashed icon). A detailed description of the system is given in reference 67.

RESULTS AND DISCUSSION

Model studies. The feasibility and reliability of the method was first evaluated on a model sample, composed of alanine, sodium 3-(trimethylsilyl)propionate-2,2,3,3-d4 (TSP) and bovine serum albumin (BSA) in buffer solution (see spectrum Fig. S2d). Alanine is a metabolite naturally present in many biological fluids, such as blood serum, and it is reported to not show any significant interaction with macromolecules.[74] TSP is often introduced as an internal standard in metabolomic studies and its interaction with macromolecules is well known.[75-76] Serum albumin is the most abundant blood protein and it is known to bind many different molecules,[77] including TSP. We used BSA as reference macromolecule (MW = 66.7 kDa, 0.5 mM). We employed highly-purified and fat-free BSA in order to avoid interference or competition arising from small impurities. Alanine and BSA were used at physiological concentrations encountered in blood serum.[78-79]

The NMRD profiles of the methyl protons of alanine and TSP are strikingly different (Fig. 3). The longitudinal relaxation rate of the methyl protons of alanine has no noticeable dependence over the magnetic field, indicating the absence of interaction with BSA. The relaxation rate is close to 0.85 s^{-1} over the entire range of magnetic fields. This uniform longitudinal relaxation rate shows that the methyl protons of alanine are in the "extreme narrowing" regime, typical for a small molecule in the absence of interactions. On the other hand, the NMRD profile for the methyl protons of TSP shows strong evidence of binding to BSA. The NMRD profile of trimethylsilyl (TMS) protons shows a first dispersion between 1 and 10 T, corresponding to a sub-nanosecond correlation time that likely corresponds to the tumbling of the free TSP with a correlation time τ_c^F. A second, stronger dispersion is observed between 30 mT and 0.3 T, and is the signature of binding of TSP to BSA, characterized by a correlation time τ_c^B.
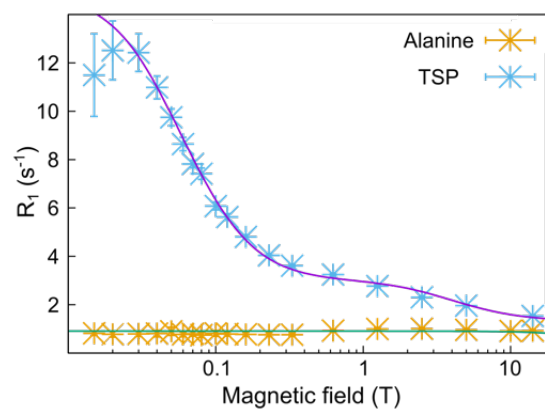

Figure 3. NMRD profiles for the methyl protons of TSP (blue crosses) and alanine (orange crosses) in the model sample. Fitted-model curves are shown as solid line for TSP (purple) and alanine (green). Equations for model curves are reported in the SI section 3 and 4.

The quantitative analysis of the two NMRD profiles was performed with molecule-specific models. Models and experiments are in excellent agreement (SI section 3 and 4). For alanine, only dipolar interactions between methyl group protons were considered and the self-rotation of the methyl group was assumed

to be infinitely fast, the population of the free form of alanine was set to $p^F = 1$. The results from the fitting revealed a correlation time of 36 ± 5 ps for the overall tumbling of alanine. For TSP, we considered the measured relaxation rates to be a weighted average between the longitudinal relaxation rates in the free and bound forms (Eq. 1). A very simple model is sufficient to reproduce the experimental NMRD profile of TSP (Fig. 3). In this model we assume infinitely fast rotation of methyl and TMS groups for the free molecules, but TMS rotation is considered to be hindered in the bound state. The order parameters are imposed by geometry.[80] Finally, we consider the limit where the population of the bound state p_B << 1. Models with additional parameters are presented as supporting information (section 4), selection based on Akaike Information Criteria[81] favored the simplest model.

Using this model, we found that the global rotational correlation time for free TSP is τ_c^F = 0.52 ± 0.03 ns and the rotational correlation time of the TSP-BSA complex is τ_c^B = 39.4 ± 1.9 ns. This is in very good agreement with an estimation of the rotational correlation time of BSA of 40 ns obtained by Ferrer *et al.*[82] by extrapolation of experimental data to 1 cP and 20°C. Overall diffusion of BSA is not expected to be isotropic: the diffusion tensor of BSA is estimated by HYDRONMR[83] to a harmonic mean correlation time τ_c^{hm} = 44.5 ns, with effective correlation times, depending on the orientation in the diffusion tensor, that vary between 41.7 ns and 47.8 ns (SI section 9). In this calculation we have assumed that the effective, microscopic, viscosity is that of the solvent,[84] which for water at 25°C is 0.89 cP.[85] Note that HYDRONMR calculations do not include any contribution of the internal mobility in the complex. Slow internal motions are expected to lower the apparent value of τ_c^B as compared to a fully rigid case, which might explain why the value of the correlation time τ_c^B is at the lower bound of the range predicted by HYDRONMR.
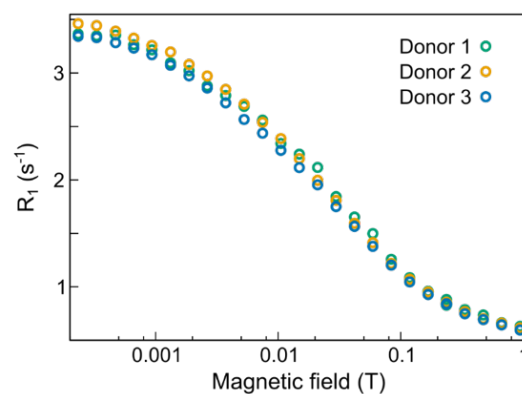

Figure 4. 1H NMRD of three serum samples from three different donors obtained by fast field-cycling relaxometry at 25°C. The analysis of the three profiles with a distribution of correlation times is described in Table S3 (SI section 5).

Metabolite binding in human serum. In order to demonstrate the potential of HRR, we have investigated interactions of metabolites with proteins in human blood serum. Blood serum is commonly investigated by metabolomics, as it contains biomarkers of great interest for clinical tests.[86] Proteins are also abundant in blood serum, making it a perfect target for discovering and measuring metabolite-protein interactions. Protein concentrations are widely distributed from 10^{-12} to 10^{-3} M, many of which are around 10^{-6} M or above (see Figure 7 and Table S5).[1, 87-94] The molecular weights of serum proteins span several orders of magnitude, from thousands of Da to the MDa range, corresponding to rotational correlation time from a few ns to a few μs. In addition, blood serum has favorable properties for methodological developments: it is self-buffered and has a stable composition, thus allowing for long experiments with satisfactory sample preservation.[95]

Experiments were carried out on blood serum samples from three healthy donors. In order to evaluate the ability of relaxometry to probe the size distribution of macromolecules in blood serum, we measured NMRD profiles on the three serum samples by FFC relaxometry, which has currently a broader range of accessible fields than HRR but no resolution. In the present case, the FFC signal is dominated by water. Yet. FFC relaxometry has been shown
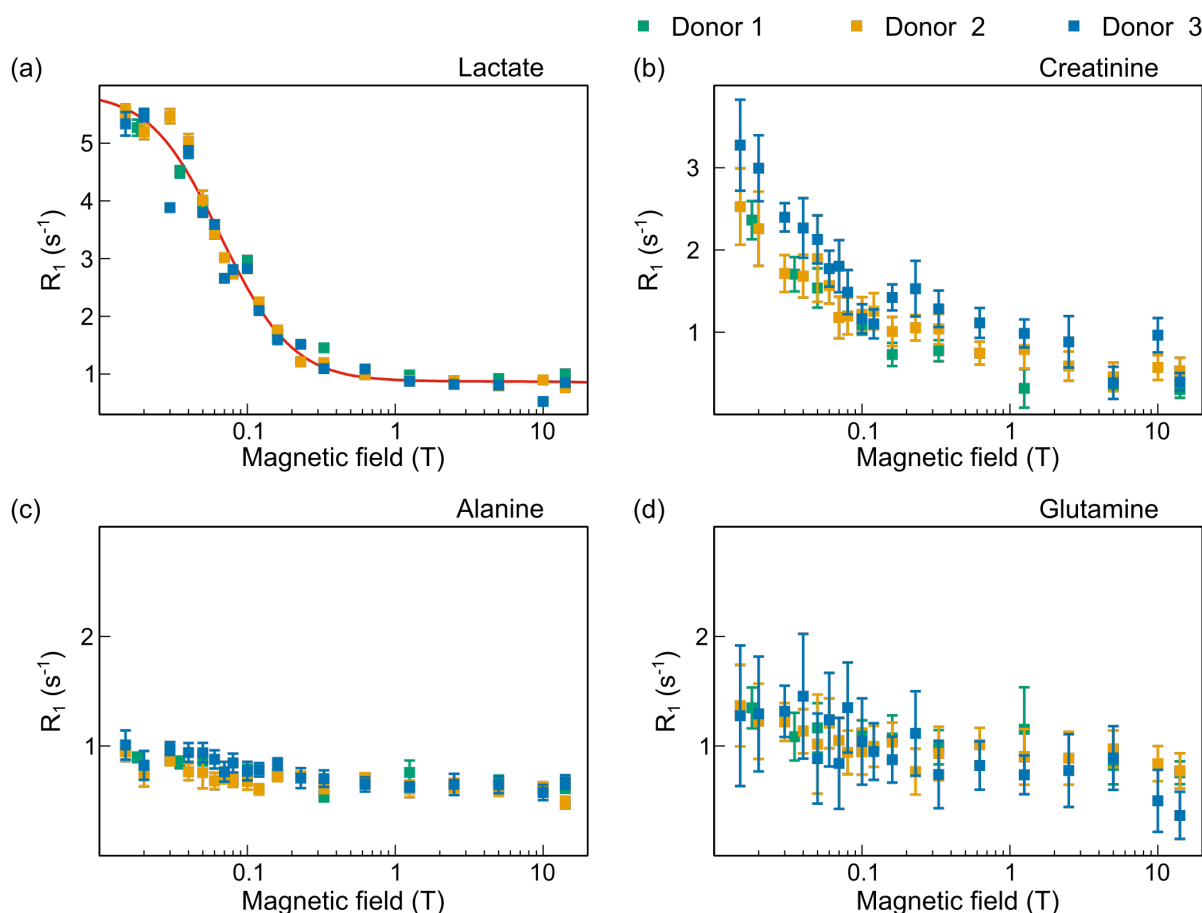
Figure 5. Proton NMRD profiles of (a) lactate (1.24 ppm), (b) creatinine (2.94 ppm), (c) alanine (1.38 ppm), and (d) glutamine (2.37 ppm) of the same three serum samples in Fig. 4. As in Figure 4, relaxation rates for the blood serum of donor 1, 2 and 3 are shown in green, yellow and blue, respectively. The fit of the NMRD profile of lactate for donor 2 is shown in (a).

to be able to probe correlation times up to the low μs range.[71] The NMRD profiles of serum samples (Fig. 4) from different donors were very similar, with variations of relaxation rates of 5% at most. The analysis of NMRD profiles (Table S3) shows contributions of correlation times between *ca.* 10 ns and *ca.* 1 μs, which is in good agreement with the size distribution of the proteins present in serum (Figures 7, S10 and Table S3).

We have previously demonstrated that high-quality spectra could be obtained with HRR on small macromolecules.[67, 80, 96] Yet, recording spectra of small molecules in complex mixtures is even more demanding in terms of resolution. Nevertheless, we clearly identified 15 metabolites as suitable targets for HRR analysis on a 1H NMR spectrum (see Fig. S2a-c). The only adaptation of a typical so-called 1D-NOESY experiment used in metabolomics[97-99] is

the addition of a WATERGATE element[100-101] for the suppression of the water signal, as the polarization of water builds up during the shuttle transfers, relaxation time, and especially the rather long stabilization delay at high field just before acquisition τ_{st-HF} = 250 ms. Here, we show the NMRD profiles of four representative metabolites in order to show different signatures of interactions with proteins (Fig. 5). The measured relaxation rates are very similar in the three serum samples for each metabolite, which reflects the expected similar compositions of serum in healthy donor.

The NMRD profile of lactate shows evidence of an interaction with macromolecules in serum (Fig. 5a). Importantly, we observe an inflection of the NMRD profile at the lowest magnetic fields, which indicates that a quantitative analysis is possible. The analysis of the NMRD

profile of lactate provides the overall rotation correlation time of the complex, hence, an estimation of the size of the complex (SI section 7). Using Equations 1-4 (SI section 3.1), we characterized the rotational dynamics of the free and bound forms of lactate (Table 1). The rotational diffusion correlation time of free lactate τ_c^F ranges between 22.8 and 35 ps, and the correlation time of the complex τ_c^B between 32.0 and 35.2 ns. The values of the parameters, particularly the product of the dipolar constant and population of the bound state $A_B p_B$, as well as the correlation time for the complex τ_c^B, are remarkably reproducible across samples of different donors. The interaction of lactate with human serum albumin (HSA) has been previously reported[74, 102-103] and HSA is the most abundant protein in serum, therefore we can assume that lactate is prevalently binding to HSA. Analogously to our model sample with BSA and TSP, we can consider that serum is diluted enough to not cause any variation in the microscopic viscosity,[84] and use HYDRONMR[83] to estimate the diffusion tensor of HSA. The estimated harmonic mean of the correlation time is 47.8 ns, with a minimum of 44.0 ns and a maximum of 51.4 ns depending on the orientation in the molecular frame (SI section 9). As mentioned above, there are several reasons for the discrepancy between our measurement and HYDRONMR calculation. Rotational anisotropy and internal motion in the protein could be significant, as well as the possible interaction of lactate with smaller proteins which are present in serum at a relatively high concentration (see Table S5 and Fig. 7 and S10).

Table 1 Parameters of the model obtained from the analysis of the NMRDs profile of the methyl protons of lactate in blood serum

Donor	$A_B p_B$ (10^6 s^{-2})	τ_c^F (ps)	τ_c^B (ns)
1	15.7 ±1.5	35 ± 7	32.0 ± 4.9
2	15.8 ± 0.7	22.8 ± 3.7	35.2 ± 2.5
3	15.8 ± 1.0	27 ± 6	34.7 ± 4.2

By contrast, alanine, glutamine (Fig. 5c-d) as well as glucose and glycine (Fig. S11) have nearly flat NMRD profile. They show very weak dispersions comparable to the experimental errors in relaxation rates. The analysis of the NMRD profiles of alanine and glutamine estimates the correlation time for tumbling τ_c to be between 0.08 ns and 0.10 ns. These results are close to our expectation for small molecules in serum, and in good agreement with the literature.[104]

The NMRD profiles of a few more metabolites, such as creatinine (Fig. 5b) and isoleucine (Fig. S11) indicate evidence of binding with macromolecules. In the case of creatinine, however, we can observe some systematic differences between sample 3 and the other two samples. Unfortunately, we could not obtain reliable quantitative analyses of these NMRD profiles, due to low precision and the possibly incomplete determination of the spectral density function (the maximum relaxation rate is clearly not reached even at the lowest field of measurement). Nevertheless, the binding of creatinine to HSA has been reported and none of the major endogenous metabolites are known to compete with it.[105] If we consider that this interaction is weak, the partial dispersion profile is compatible with the binding of creatinine to HSA, within the large error bars due to the low concentration of creatinine (about 80 µM). This hypothesis was confirmed by measurements of the transverse relaxation rate of the creatinine methyl protons in a buffer, with and without BSA (SI section 6). However, we cannot rule out additional interactions of creatinine with other proteins.

Binding competition between metabolites and TSP. Binding competition is an indirect method to characterize a broader set of interactions, in particular tighter interactions, than those accessible by HRR. We have shown that TSP is binding to BSA, and investigated the interaction of lactate to human serum albumin (HSA). Barrilero et al.[76] have shown evidence for competition between lactate and TSP for

binding to HSA. As a proof of concept, we investigated this binding competition by HRR. We prepared two blood serum samples (donor 1) with and without TSP (14 mM) and we recorded the NMRD profile of lactate and creatinine (Fig. 6). The NMRD profiles of creatinine for the two samples are similar (Fig. 6a), as expected from a study by Barrilero *et al.*[76] On the contrary, the proton longitudinal relaxation rates of the methyl group of lactate are much lower in the sample with TSP, confirming the binding competition between the two molecules for HSA (Fig. 6b). Interestingly, the rotational correlation times for the free and bound form of lactate are identical in the samples with and without TSP (Table 2). The only difference between the two NMRD profiles of lactate is found to originate from the different values of the parameter $A_B p_B$, which decreased from $15.7 \pm 1.5\ 10^6\ s^{-2}$ in the absence of TSP to $5.9 \pm 0.4\ 10^6\ s^{-2}$ upon addition of TSP. This decrease by a factor of 2.7 $\pm$ 0.3 in the presence of TSP can be assigned to a change in the bound fraction, which decreases by more than 60% in the presence of 14 mM of TSP. HRR provides a clear evidence of binding competition, and the analysis of the NMRD profiles leads to a quantitative determination of the changes in binding populations.

Table 2 Parameters from the analysis of the NMRDs of lactate in serum samples with and without TSP.

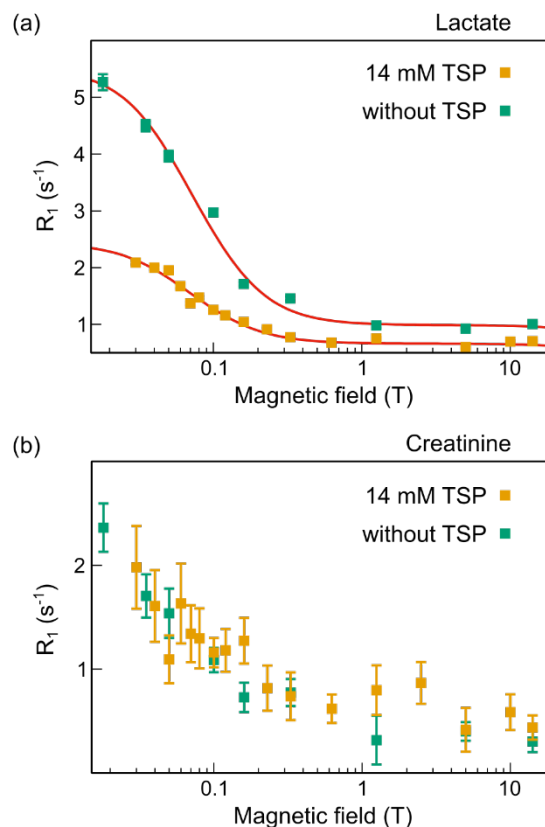| Sample	$A_B p_B$ (10^6 s^{-2})	τ_c^F (ps)	τ_c^B (ns)
With 14 mM TSP	5.9 ± 0.4	33 ± 3	33.3 ± 4.8
Without TSP	15.7 ± 1.5	35 ± 7	32.0 ± 4.9

Figure 6. NMRD profiles of the methyl protons of (a) creatinine and (b) lactate from blood serum samples of donor 1, with 14 mM of TSP (yellow squares) and without TSP (green squares). The red lines are the results of the fit with Equations S6, providing parameters presented in Table 2.

Discussion. In blood serum, about 30 metabolites are detectable by NMR without any sample purification and 35 proteins have concentrations above 1 µM, which should be accessible to the current method.[26, 78, 106-109] This means that potentially over 1000 different interactions could be probed by HRR. Here, we identified fifteen metabolites by 1D proton NMR on our prototype and we show NMRD profiles for four of them: lactate, creatinine, glutamine and alanine. The experiments were carried out on three different serum samples from healthy donors and the results were uniform for all of them. The NMRD profiles of the metabolites show that for some of them (i.e. lactate and creatinine) there is a significant interaction with macromolecules, whereas others (i.e. glutamine and alanine) have little to no interaction with proteins. For lactate, we obtained a correlation time of its bound form,

$\tau_c^B = 34.0 \pm 3.9$ ns, which is, within a reasonable error margin, compatible with the one estimated by HYDRONMR for HSA. Note that decay rates in high-resolution relaxometry experiments deviate from longitudinal relaxation rates by as much as 15% in proteins.[80, 110-111] Here, our analysis assumes that the decay rates are the longitudinal relaxation rates, which should minimally impact the obtained values of correlation times.[80] Finally, we were also able to identify competitive binding of small molecules to serum albumin in human blood serum, which could prove to be a new approach for performing fragment-based drug design directly in a complex biological fluid.

HRR benefits from several advantages as compared to other methods to investigate MPIs. First, there is no separation step during sample preparation: experiments are directly performed on the serum obtained from blood by standard procedures. Second, relaxometry is able to probe weak transient interactions, which are extremely difficult to detect by existing methods.[42-43] Third, the analysis is quantitative and provides information to identify the protein interacting with the observed metabolite. Currently, the range of magnetic field that we can probe allows to quantify the rotational correlation time of a complex as slow as ~50 to 100 nanoseconds. The determination of this correlation time provides an estimate of the size of the complexes, hence of the size of the proteins that interact with a given metabolite (SI section 7).[112] The accuracy of correlation times determined by HYDRONMR is within about 10%.[83] If we estimate the error on the correlation times given by HRR to be around 10%, we can consider the agreement of HYDRONMR and HRR within a range of ±20%. Our current HRR system is less sensitive than a state-of-the-art NMR system (10% of the sensitivity of a room-temperature probe). We estimate the sensitivity limit for a quantitative analysis to 100 µM for metabolites and 1 µM for the complex (for ~1% of bound metabolite).

Considering only serum proteins that are present in concentrations above 1 µM, the correlation times within a ±20% range indicate only a few interacting proteins as potential candidates. The distribution of correlation times is not uniform so that the number of candidates in this range varies from 1 to 8, depending on the value of the correlation time (Fig. 7b). Note that the amplitude of the relaxation dispersion is proportional to the bound fraction and the correlation time of the complex. Thus, the minimal bound faction for detection is expected to be inversely proportional to the size of the complex.

The information provided by HRR can be expected to be augmented by combination with other NMR methods, in particular saturation transfer difference (STD). STD directly probes the parts of a small molecule or ligand in direct contact with a macromolecule,[113] providing a structural information highly complementary to HRR results. In addition, the combined quantitative analysis of HRR and STD, with tools such as the Complete Relaxation and Conformational Exchange Matrix (CORCEMA),[114] may help determine the amplitude of intermolecular dipole-dipole interactions (structural information) and the bound fraction (thermodynamics).

We present here a proof of concept with a technology that is not yet ready for high throughput. The current apparatus requires tedious sample preparation, while this step is often automated for high-throughput metabolomic studies.[30] In addition, the current sensitivity is well below the state of the art (10% of the sensitivity of a room-temperature probe). Increasing the throughput would require high sensitivity and automation, which could be achieved with sample shuttle designs that use regular NMR tubes.[66]
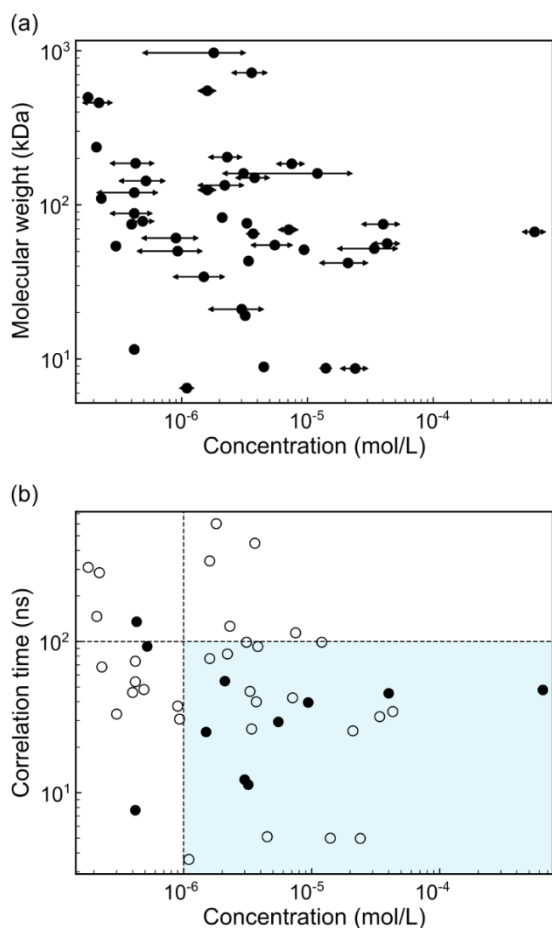
Figure 7. (a) Distribution of molecular weights and concentrations of human serum proteins. The arrow spans indicate the known concentration variability of each protein. (b) Distribution of correlation times and concentrations of human serum proteins. The solid black symbols indicate the harmonic mean of the correlation times of proteins calculated using HYDRONMR. The open symbols indicate correlation times of proteins calculated using a simple linear relationship between molecular weight and correlation time (see Eq. S8). The dashed lines represent estimates of the limits of detection of our current setup (imposed by sensitivity and range of accessible magnetic fields), and the light blue area represents the currently accessible region.

CONCLUSION

We have introduced an approach based on high-resolution relaxometry to investigate metabolite-protein interactions in biological fluids. We have measured with HRR and analyzed site-specific proton longitudinal relaxation rates in metabolites over three orders of magnitude of magnetic field (from 15 mT to 14 T). The method was first established on a model sample, containing alanine, TSP and BSA. We clearly identified the weak binding of TSP to BSA and obtained an estimate of the rotational correlation time of BSA in good agreement with what is expected from its molecular weight and the literature. We demonstrated that this method could be used in a biological fluid such as human blood serum. We used HRR to determine the NMRD profiles of lactate, creatinine, alanine and glutamine. We found clear evidence that, in serum, lactate and creatinine interact weakly with macromolecules, i.e. proteins, whereas alanine and glutamine do not. The quantitative analyses of the NMRD profiles of lactate provided nearly identical estimates of the rotational correlation time of the complex in the blood of three different healthy donors. These estimates are in good agreement with the known interaction of lactate with HSA but could also reflect weak binding to a smaller protein. We also demonstrated that the interactions could be investigated indirectly through a binding competition experiment, which opens the way for the investigation of strong interactions by HRR. Upon addition of TSP to blood serum, the dispersion amplitude of lactate is reduced and the variation of the bound fraction of lactate was quantified. Our investigation demonstrates the potential of high-resolution relaxometry as a non-invasive and quantitative analytical tool for biological fluids. With HRR, NMR can become a powerful tool for the investigation of metabolite-protein interactions for interactomics and, in general, for the analysis of small-molecule–macromolecule interactions in complex media, for chemical and pharmaceutical applications.

MATERIALS AND METHODS

Samples preparation. Each analyzed sample was placed in a custom-sized NMR tube made of amorphous quartz, with an active volume of ~60 μL, sealed with glue (Eleco-EFD Vitralit® 2009 F) and capped with specifically designed polyimide tops, which fit the probe cavity and help absorbing shocks upon shuttling.

The model sample contains 0.5 mM alanine, 50 mM TSP and 0.5 mM BSA, as a substitute for human serum albumin. All compounds were dissolved in a phosphate buffer (pH 7.4, 35 mM Na2HPO4, 0.58 mM NaN3 in H2O/D2O 90/10 (v/v)). All compounds were purchased from Sigma Aldrich – Merck.

The serum samples were collected, prepared and stored according to standard metabolomic procedures.95 Before being transferred to a shuttle tube, frozen samples were thawed at room temperature and homogenized with an agitator. 5% v/v of D2O was added for lock purposes and they were sealed directly into shuttle tubes.

The serum sample with TSP as competing molecule contained 30% (v/v) buffer (pH 7.4, 35 mM Na2HPO4, 0.58 mM NaN3, and 46 mM TSP in H2O/D2O 90/10 (v/v)). The final concentration of TSP in this serum sample was then 14 mM.

NMR spectroscopy. HRR experiments were carried out on a Bruker Avance III HD spectrometer operating at 14.1 T, with a shuttle apparatus and a 3.2 mm triple-resonance probe with a z-axis gradient.[67] A temperature calibration sample contains deuterated acetic acid buffer (50 mM) and 7% D2O was used to perform blank relaxation experiment by reproducing real experimental conditions, including shuttle transfers, relaxation at the low field position, etc. Then the temperature was calibrated using deuterium chemical shift difference between acetic acid and water (OD) signals. We ensured that NMR measurements were performed at (298.0 ± 0.2) K for all delays at all fields.[115] The pulse sequence for the high-resolution relaxometry experiment was adapted from a standard so-called 1D NOESY, by adding a relaxation delay at low field and WATERGATE[100-101] blocks (SI section 1). [1]H longitudinal relaxation rates were measured at different magnetic field magnitudes over 3 orders of magnetic strength from 14.1 T down to 15 mT (14.1, 10.0, 5.0, 2.5, 1.25, 0.625, 0.33,

0.23, 0.16, 0.12, 0.10, 0.08, 0.07, 0,06, 0.05, 0.04, 0.03, 0.02, 0.015 T). Each relaxation decay was characterized by 7 relaxation delays (from 0.001 s to a maximum of 1 s depending on the field). The number of scans varies between 288 and 2304 depending on the field for sufficient signal to noise ratios.

HRR Data analysis. HRR experiments were processed using NMRPipe using the solvent filter option and a sine-bell apodization function.[116] Signals of individual molecule were measured by summing up intensities over a chosen interval. Baseline correction was applied after Fourier transform of the FID. For minor baseline corrections, the averaged intensities at the extremities of the chosen intervals were used to define a linear function subtracted from the spectra. The peak for lactate overlaps with a large signal of lipids aliphatic protons and baseline correction was applied using the NMRPipe[112] POLY function. The intensity uncertainty was estimated from signal-free regions of the spectra. Intensity decays were fitted using a mono-exponential decay function, and errors in the relaxation rate evaluated by Monte-Carlo analysis in Octave.[117] The NMR dispersion profile were analyzed to yield parameters of the models using 120,000 steps Markov-Chain Monte-Carlo (MCMC) using Octave.[113] The first 25,000 stabilization points were removed from the analysis. The MCMC trajectory was then analyzed to extract the optimized parameters, their confidence intervals, and visualize correlations between the parameters.

FFC NMRD profiles. Water ^{1}H FFC NMRD profiles were obtained by measuring the water proton relaxation rates, R1, as a function of the applied magnetic field. The profiles were measured with a SPINMASTER2000 fast field cycling relaxometer (Stelar, Mede (PV), Italy) operating in the 0.01–40 MHz proton Larmor frequency range. The measurements are affected by an error of about ±1%, when fitted to a monoexponential decay/recovery of the magnetization in the field cycling experiment. The profiles were fitted using the sum of the

contributions from the homonuclear dipole-dipole relaxation with four different correlation times (SI section 5).

ASSOCIATED CONTENT

Supporting Information. Information on pulse sequences and examples of relaxation decays; comparison of models for the analysis of NMRD profiles; analysis of fast-field cycling NMRD profiles; measurement of high-field transverse relaxation rates of methyl protons in creatinine; correlation of molecular weight and rotational correlation times from HYDRONMR; table of proteins in blood serum; hydrodynamics calculations with HYDRONMR; NMRD profiles for additional metabolites. This material is available free of charge via the Internet at http://pubs.acs.org/doi/xxxxxxx"

AUTHOR INFORMATION

Corresponding Author

Fabien Ferrage – Laboratoire des Biomolécules, LBM, Département de chimie, École normale supérieure, PSL University, Sorbonne Université, CNRS, 75005 Paris, France;

orcid.org/0000-0002-4738-1723;

Email: fabien.ferrage@ens.psl.eu

Claudio Luchinat – Magnetic Resonance Center (CERM) and Department of Chemistry "Ugo Schiff", University of Florence, and Consorzio Interuniversitario Risonanze Magnetiche MetalloProteine (CIRMMP), Sesto Fiorentino, Italy; orcid.org/0000-0003-2271-8921; Email: luchinat@cerm.unifi.it

Present Addresses

Central European Institute of Technology, Masaryk University, Kamenice 5, 625 00 Brno, Czech Republic

† Department for NMR-based Structural Biology, Max Planck Institute for Biophysical Chemistry, Am Faßberg 11, 37077 Göttingen, Germany

Author Contributions

The manuscript was written through contributions of all authors. All authors have given approval to the final version of the manuscript.

Notes

J.-M. T. and T. M. are employees of Bruker Biospin. The authors declare no other conflict of interest.

ABBREVIATIONS

PPI, protein-protein interactions; MPI, metabolite-protein interactions; FFC, fast field-cycling; HRR, high-resolution relaxometry; NMRD, NMR relaxation dispersion; TSP, 3-(trimethylsilyl)propionate-2,2,3,3-d4; BSA, bovine serum albumin; TMS, trimethylsilyl; HSA, human serum albumin;

REFERENCES

1. Bhagavan, N. V., *Medical biochemistry (Fourth Edition)*. Academic press: San Diego, 2002.

2. Burton, C.; Kaczmarski, R.; Glew, R.; Rosenthal, M., Glucose 6-phosphate dehydrogenase deficiency and oxidative hemolysis. *Clinical studies in medical biochemistry* **2007,** *1*, 123-133.

3. Weckwerth, W., Metabolomics in systems biology. *Annual review of plant biology* **2003,** *54* (1), 669-689.

4. Idle, J. R.; Gonzalez, F. J., Metabolomics. *Cell metabolism* **2007,** *6* (5), 348-351.

5. Lindon, J. C.; Holmes, E.; Nicholson, J. K., Metabonomics in pharmaceutical R & D. *The FEBS journal* **2007,** *274* (5), 1140-1151.

6.   Cabrera, W. L.; Knapp, J. S., *Metabolomics: metabolites, metabonomics, and analytical technologies*. Nova Science Publishers: 2011.

7.   Patti, G. J.; Yanes, O.; Siuzdak, G., Innovation: Metabolomics: the apogee of the omics trilogy. *Nature reviews Molecular cell biology* **2012,** *13* (4), 263.

8.   Blackstock, W. P.; Weir, M. P., Proteomics: quantitative and physical mapping of cellular proteins. *Trends in biotechnology* **1999,** *17* (3), 121-127.

9.   Fields, S., Proteomics in genomeland. *Science* **2001,** *291* (5507), 1221-1224.

10.   Patterson, S. D.; Aebersold, R. H., Proteomics: the first decade and beyond. *Nature genetics* **2003,** *33* (3s), 311.

11.   Hanash, S., Disease proteomics. *Nature* **2003,** *422* (6928), 226.

12.   Graves, P. R.; Haystead, T. A. J., Molecular Biologist's Guide to Proteomics. *Microbiology and Molecular Biology Reviews* **2002,** *66* (1), 39-63.

13.   Madsen, R.; Lundstedt, T.; Trygg, J., Chemometrics in metabolomics—a review in human disease diagnosis. *Analytica chimica acta* **2010,** *659* (1-2), 23-33.

14.   Emwas, A.-H. M.; Salek, R. M.; Griffin, J. L.; Merzaban, J., NMR-based metabolomics in human disease diagnosis: applications, limitations, and recommendations. *Metabolomics* **2013,** *9* (5), 1048-1072.

15.   Nicholson, J. K.; Wilson, A. D., High resolution proton magnetic resonance spectroscopy of biological fluids. *Progress in NMR spectroscopy* **1989,** *21*, (4-5), 449-501.

16.   Bottomley, P. A., Human in vivo NMR spectroscopy in diagnostic medicine: clinical tool or research probe? *Radiology*, **1989,** *170*, (1), 1-15.

17.   Foxall, P. J. D.; Mellotte, G. J.; Bending, M. R.; Lindon, J. C.; Nicholson, J. K., NMR as a novel approach to the monitoring of renal transplant function. *Kidney International*, **1993,** *43*, (1), 234-245.

18.   Nicholson, J. K.; Lindon, J. C.; Holmes, E., 'Metabonomics': understanding the metabolic responses of living systems to pathophysiological stimuli via multivariate statistical analysis of biological NMR spectroscopic data. *Xenobiotica*, **1999,** *29*, (11), 1181-1189.

19.   Timbrell, J. A., Biomarkers in toxicology. *Toxicology*, **1998,** *129*, (1), 1-12.

20.   Lindon, J. C.; Nicholson, J. K.; Holmes, E; Everett, J. R., Metabonomics: metabolic processes studied by NMR spectroscopy of biofluids. *Concepts in Magnetic Resonance*, **2000,** *12*, (5), 289-320.

21.   Robertson, D. G.; Reily, M. D.; Sigler, R. E.; Wells, D. F.; Paterson, D. A.; Braden, T. K., Metabonomics: evaluation of nuclear magnetic resonance (NMR) and pattern recognition technology for rapid *in vivo* screening of liver and kidney toxicants. *Toxicological Sciences*, **2000,** *57*, (2), 326-337.

22.   Holmes, E.; Nicholls, A. W.; Lindon, J. C.; Connor, S. C.; Connely, J. C.; Haselden, J. N.; Damment, S. J. P.; Spraul, M.; Neidig, P.; Nicholson, J. K., Chemometric models for toxicity classification based on NMR spectra of biofluids. *Chemical Research in Toxicology*, **2000,** *13*, (6), 471-478.

23.   Yee, A.; Chang, X.; Pineda-Lucena, A.; Wu, B.; Semesi, A.; Le, B.; Ramelot, T.; Lee, G. M.; Bhattacharyya, S.; Gutierrez, P., An NMR approach to structural proteomics. *Proceedings of the National Academy of Sciences* **2002,** *99* (4), 1825-1830.

24.   de Graaf, R. A.; Behar, K. L., Quantitative 1H NMR spectroscopy of blood plasma metabolites. *Analytical chemistry* **2003,** *75* (9), 2100-2104.

25.   Wishart, D. S., Quantitative metabolomics using NMR. *TrAC trends in analytical chemistry* **2008,** *27* (3), 228-237.

26.   Gowda, G. N.; Raftery, D., Can NMR solve some significant challenges in metabolomics? *Journal of Magnetic Resonance* **2015,** *260*, 144-160.

27.   Dona, A. C.; Kyriakides, M.; Scott, F.; Shephard, E. A.; Varshavi, D.; Veselkov, K.; Everett, J. R., A guide to the identification of metabolites in NMR-based metabonomics/metabolomics experiments. *Computational and structural biotechnology journal* **2016,** *14*, 135-153.

28.   Nagana Gowda, G.; Raftery, D., Recent advances in NMR-based metabolomics. *Analytical chemistry* **2016,** *89* (1), 490-510.

19.   Shin, J.; Lee, W.; Lee, W., Structural proteomics by NMR spectroscopy. *Expert review of proteomics* **2008,** *5* (4), 589-601.

30.   Vignoli, A.; Ghini, V.; Meoni, G.; Licari, C.; Takis, P. G.; Tenori, L.; Turano, P.; Luchinat, C., High-Throughput Metabolomics by 1D NMR. *Angewandte Chemie International Edition* **2019,** *58* (4), 968-994.

31.   Takis, P. G.; Ghini, V.; Tenori, L.; Turano, P.; Luchinat, C., Uniqueness of the NMR approach to metabolomics. *TrAC Trends in Analytical Chemistry* **2019,** *120*, 115300.

32.   Giraudeau, P., NMR-based metabolomics and fluxomics: developments and future prospects. *Analyst* **2020,** *145* (7), 2457-2472.

33.   Vidal, M.; Cusick, M. E.; Barabási, A.-L., Interactome networks and human disease. *Cell* **2011,** *144* (6), 986-998.

34.   Luck, K.; Sheynkman, G. M.; Zhang, I.; Vidal, M., Proteome-scale human interactomics. *Trends in biochemical sciences* **2017,** *42* (5), 342-354.

35. Nooren, I. M.; Thornton, J. M., Diversity of protein–protein interactions. *The EMBO journal* **2003,** *22* (14), 3486-3492.

36. Stelzl, U.; Worm, U.; Lalowski, M.; Haenig, C.; Brembeck, F. H.; Goehler, H.; Stroedicke, M.; Zenkner, M.; Schoenherr, A.; Koeppen, S., A human protein-protein interaction network: a resource for annotating the proteome. *Cell* **2005,** *122* (6), 957-968.

37. Ryan, D. P.; Matthews, J. M., Protein–protein interactions in human disease. *Current opinion in structural biology* **2005,** *15* (4), 441-446.

38. Oti, M.; Snel, B.; Huynen, M. A.; Brunner, H. G., Predicting disease genes using protein–protein interactions. *Journal of medical genetics* **2006,** *43* (8), 691-698.

39. Ewing, R. M.; Chu, P.; Elisma, F.; Li, H.; Taylor, P.; Climie, S.; McBroom-Cerajewski, L.; Robinson, M. D.; O'Connor, L.; Li, M.; Taylor, R.; Dharsee, M.; Ho, Y.; Heilbut, A.; Moore, L.; Zhang, S.; Ornatsky, O.; Bukhman, Y. V.; Ethier, M.; Sheng, Y.; Vasilescu, J.; Abu-Farha, M.; Lambert, J.-P.; Duewel, H. S.; Stewart, I. I.; Kuehl, B.; Hogue, K.; Colwill, K.; Gladwish, K.; Muskat, B.; Kinach, R.; Adams, S.-L.; Moran, M. F.; Morin, G. B.; Topaloglou, T.; Figeys, D., Large-scale mapping of human protein-protein interactions by mass spectrometry. *Molecular systems biology* **2007,** *3:89*, 1-17.

40. Kazemzadeh, L.; Kamdar, M. R.; Beyan, O. D.; Decker, S.; Barry, F., LinkedPPI: enabling intuitive, integrative protein-protein interaction discovery. In *Proceedings of the 4th International Conference on Linked Science - Volume 1282*, CEUR-WS.org: Riva del Garda, Italy, 2014; pp 48–59.

41. Gordon, D. E.; Jang, G. M.; Bouhaddou, M.; Xu, J.; Obernier, K.; White, K. M.; O'Meara, M. J.; Rezelj, V. V.; Guo, J. Z.; Swaney, D. L.; Tummino, T. A.; Hüttenhain, R.; Kaake, R. M.; Richards, A. L.; Tutuncuoglu, B.; Foussard, H.; Batra, J.; Haas, K.; Modak, M.; Kim, M.; Haas, P.; Polacco, B. J.; Braberg, H.; Fabius, J. M.; Eckhardt, M.; Soucheray, M.; Bennett, M. J.; Cakir, M.; McGregor, M. J.; Li, Q.; Meyer, B.; Roesch, F.; Vallet, T.; Mac Kain, A.; Miorin, L.; Moreno, E.; Naing, Z. Z. C.; Zhou, Y.; Peng, S.; Shi, Y.; Zhang, Z.; Shen, W.; Kirby, I. T.; Melnyk, J. E.; Chorba, J. S.; Lou, K.; Dai, S. A.; Barrio-Hernandez, I.; Memon, D.; Hernandez-Armenta, C.; Lyu, J.; Mathy, C. J. P.; Perica, T.; Pilla, K. B.; Ganesan, S. J.; Saltzberg, D. J.; Rakesh, R.; Liu, X.; Rosenthal, S. B.; Calviello, L.; Venkataramanan, S.; Liboy-Lugo, J.; Lin, Y.; Huang, X.-P.; Liu, Y.; Wankowicz, S. A.; Bohn, M.; Safari, M.; Ugur, F. S.; Koh, C.; Savar, N. S.; Tran, Q. D.; Shengjuler, D.; Fletcher, S. J.; O'Neal, M. C.; Cai, Y.; Chang, J. C. J.; Broadhurst, D. J.; Klippsten, S.; Sharp, P. P.; Wenzell, N. A.; Kuzuoglu-Ozturk, D.; Wang, H.-Y.; Trenker, R.; Young, J. M.; Cavero, D. A.; Hiatt, J.; Roth, T. L.; Rathore, U.; Subramanian, A.; Noack, J.; Hubert, M.; Stroud, R. M.; Frankel, A. D.; Rosenberg, O. S.; Verba, K. A.; Agard, D. A.; Ott, M.; Emerman, M.; Jura, N.; von Zastrow, M.; Verdin, E.; Ashworth, A.; Schwartz, O.; d'Enfert, C.; Mukherjee, S.; Jacobson, M.; Malik, H. S.; Fujimori, D. G.; Ideker, T.; Craik, C. S.; Floor, S. N.; Fraser, J. S.; Gross, J. D.; Sali, A.; Roth, B. L.; Ruggero, D.; Taunton, J.; Kortemme, T.; Beltrao, P.; Vignuzzi, M.; García-Sastre, A.; Shokat, K. M.; Shoichet, B. K.; Krogan, N. J., A SARS-CoV-2 protein interaction map reveals targets for drug repurposing. *Nature* **2020,** *583* (7816), 459-468.

42. Piazza, I.; Kochanowski, K.; Cappelletti, V.; Fuhrer, T.; Noor, E.; Sauer, U.; Picotti, P., A Map of Protein-Metabolite Interactions Reveals Principles of Chemical Communication. *Cell* **2018,** *172* (1), 358-372.e23.

43. Diether, M.; Nikolaev, Y.; Allain, F. H.; Sauer, U., Systematic mapping of protein-metabolite interactions in central metabolism of Escherichia coli. *Molecular systems biology* **2019,** *15* (8), e9008-e9008.

44. Yang, G.; Li, X.; Snyder, M., Investigating metabolite–protein interactions: An overview of available techniques. *Methods* **2012,** *57* (4), 459-466.

45. Luzarowski, M.; Skirycz, A., Emerging strategies for the identification of protein-metabolite interactions. *J Exp Bot* **2019,** *70* (18), 4605-4618.

46. Li, X.; Wang, X.; Snyder, M., Systematic investigation of protein–small molecule interactions. *IUBMB Life* **2013,** *65* (1), 2-8.

47. Matsuda, R.; Bi, C.; Anguizola, J.; Sobansky, M.; Rodriguez, E.; Badilla, J.; Zheng, X.; Hage, B.; Hage, D. S., Studies of metabolite–protein interactions: A review. *Journal of Chromatography B* **2014,** *966*, 48-58.

48. Chen, A.; Shapiro, M. J., NOE Pumping: A Novel NMR Technique for Identification of Compounds with Binding Affinity to Macromolecules. *Journal of the American Chemical Society* **1998,** *120* (39), 10258-10259.

49. Mayer, M.; Meyer, B., Characterization of Ligand Binding by Saturation Transfer Difference NMR Spectroscopy. *Angewandte Chemie International Edition* **1999,** *38* (12), 1784-1788.

50. Vogtherr, M.; Peters, T., Application of NMR Based Binding Assays to Identify Key Hydroxy Groups for Intermolecular Recognition. *Journal of the American Chemical Society* **2000,** *122* (25), 6093-6099.

51. Dalvit, C.; Fogliatto, G.; Stewart, A.; Veronesi, M.; Stockman, B., WaterLOGSY as a method for primary NMR screening: Practical aspects and range of applicability. *Journal of Biomolecular NMR* **2001,** *21* (4), 349-359.

52. Meyer, B.; Peters, T., NMR Spectroscopy Techniques for Screening and Identifying Ligand Binding to Protein Receptors. *Angewandte Chemie International Edition* **2003,** *42* (8), 864-890.

53. Evans, R.; Deng, Z.; Rogerson, A. K.; McLachlan, A. S.; Richards, J. J.; Nilsson, M.; Morris, G. A., Quantitative Interpretation of Diffusion-Ordered NMR Spectra: Can We Rationalize Small Molecule Diffusion Coefficients? *Angew. Chem. Int. Ed.* **2013,** *52* (11), 3199-3202.

54. Chen, A.; Shapiro, M. J., Peer Reviewed: Affinity NMR. *Analytical Chemistry* **1999,** *71* (19), 669A-675A.

55. Johnson, C. S., Diffusion ordered nuclear magnetic resonance spectroscopy: principles and applications. *Prog. Nucl. Magn. Reson. Spectrosc.* **1999,** *34* (3-4), 203-256.

56. Kimmich, R.; Anoardo, E., Field-cycling NMR relaxometry. *Progress in Nuclear Magnetic Resonance Spectroscopy* **2004,** *44* (3-4), 257-320.

57. Bertini, I.; Gupta, Y. K.; Luchinat, C.; Parigi, G.; Schlörb, C.; Schwalbe, H., NMR spectroscopic detection of protein protons and longitudinal relaxation rates between 0.01 and 50 MHz. *Angewandte Chemie International Edition* **2005,** *44* (15), 2223-2225.

58. Luchinat, C.; Parigi, G., Collective Relaxation of Protein Protons at Very Low Magnetic Field: A New Window on Protein Dynamics and Aggregation. *Journal of the American Chemical Society* **2007,** *129* (5), 1055-1064.

59. Borsi, V.; Luchinat, C.; Parigi, G., Global and Local Mobility of Apocalmodulin Monitored through Fast-Field Cycling Relaxometry. *Biophysical Journal* **2009,** *97* (6), 1765-1771.

60. Korb, J.-P., Multiscale nuclear magnetic relaxation dispersion of complex liquids in bulk and confinement. *Prog. Nucl. Magn. Reson. Spectrosc.* **2018,** *104*, 12-55.

61. Chou, C.-Y.; Abdesselem, M.; Bouzigues, C.; Chu, M.; Guiga, A.; Huang, T.-H.; Ferrage, F.; Gacoin, T.; Alexandrou, A.; Sakellariou, D., Ultra-wide range field-dependent measurements of the relaxivity of Gd1−xEuxVO4 nanoparticle contrast agents using a mechanical sample-shuttling relaxometer. *Scientific Reports* **2017,** *7* (1), 44770.

62. Redfield, A. G., Shuttling device for high-resolution measurements of relaxation and related phenomena in solution at low field, using a shared commercial 500 MHz NMR instrument. *Magnetic Resonance in Chemistry* **2003,** *41* (10), 753-768.

63. Redfield, A. G., High-resolution NMR field-cycling device for full-range relaxation and structural studies of biopolymers on a shared commercial instrument. *Journal of biomolecular NMR* **2012,** *52* (2), 159-177.

64. Reese, M.; Türke, M.-T.; Tkach, I.; Parigi, G.; Luchinat, C.; Marquardsen, T.; Tavernier, A.; Höfer, P.; Engelke, F.; Griesinger, C.; Bennati, M., 1H and 13C Dynamic Nuclear Polarization in Aqueous Solution with a Two-Field (0.35 T/14 T) Shuttle DNP Spectrometer. *Journal of the American Chemical Society* **2009,** *131* (42), 15086-15087.

65. Krahn, A.; Lottmann, P.; Marquardsen, T.; Tavernier, A.; Türke, M.-T.; Reese, M.; Leonov, A.; Bennati, M.; Hoefer, P.; Engelke, F.; Griesinger, C., Shuttle DNP spectrometer with a two-center magnet. *Physical Chemistry Chemical Physics* **2010,** *12* (22), 5830-5840.

66. Chou, C.-Y.; Chu, M.; Chang, C.-F.; Huang, T.-h., A compact high-speed mechanical sample shuttle for field-dependent high-resolution solution NMR. *Journal of Magnetic Resonance* **2012,** *214*, 302-308.

67. Charlier, C.; Khan, S. N.; Marquardsen, T.; Pelupessy, P.; Reiss, V.; Sakellariou, D.; Bodenhausen, G.; Engelke, F.; Ferrage, F., Nanosecond Time Scale Motions in Proteins Revealed by High-Resolution NMR Relaxometry. *J. Am. Chem. Soc.* **2013,** *135* (49), 18665-18672.

68. Zhukov, I. V.; Kiryutin, A. S.; Yurkovskaya, A. V.; Grishin, Y. A.; Vieth, H.-M.; Ivanov, K. L., Field-cycling NMR experiments in an ultra-wide magnetic field range: relaxation and coherent polarization transfer. *Physical Chemistry Chemical Physics* **2018,** *20* (18), 12396-12405.

69. Roberts, M. F.; Redfield, A. G., High Resolution 31P NMR Field Cycling Probes Phospholipid Dynamics and Interactions with Phosphatidylinositol-Specific Phospholipase C. *The FASEB Journal* **2006,** *20* (4), A61-A61.

70. Pu, M.; Feng, J.; Redfield, A. G.; Roberts, M. F., Enzymology with a Spin-Labeled Phospholipase C: Soluble Substrate Binding by 31P NMR from 0.005 to 11.7 T. *Biochemistry* **2009,** *48* (35), 8282-8284.

71. Ravera, E.; Parigi, G.; Mainz, A.; Religa, T. L.; Reif, B.; Luchinat, C., Experimental Determination of Microsecond Reorientation Correlation Times in Protein Solutions. *The Journal of Physical Chemistry B* **2013,** *117* (13), 3548-3553.

72. Kim, S.; Chen, J.; Cheng, T.; Gindulyte, A.; He, J.; He, S.; Li, Q.; Shoemaker, B. A.; Thiessen, P. A.; Yu, B.; Zaslavsky, L.; Zhang, J.; Bolton, E. E., PubChem 2019 update: improved access to chemical data. *Nucleic Acids Res.* **2019,** *47* (D1), D1102-D1109.

73. Cousin, S. F.; Charlier, C.; Kaderavek, P.; Marquardsen, T.; Tyburn, J.-M.; Bovier, P.-A.; Ulzega, S.; Speck, T.; Wilhelm, D.; Engelke, F.; Maas, W.; Sakellariou, D.; Bodenhausen, G.; Pelupessy, P.; Ferrage, F., High-resolution two-field nuclear

magnetic resonance spectroscopy. *PCCP* **2016,** *18* (48), 33187-33194.

74. Bell, J. D.; Brown, J. C. C.; Kubal, G.; Sadler, P. J., NMR-invisible lactate in blood plasma. *FEBS Letters* **1988,** *235* (1), 81-86.

75. Kriat, M.; Confort-Gouny, S.; Vion-Dury, J.; Sciaky, M.; Viout, P.; Cozzone, P. J., Quantitation of metabolites in human blood serum by proton magnetic resonance spectroscopy. A comparative study of the use of formate and TSP as concentration standards. *NMR in Biomedicine* **1992,** *5* (4), 179-184.

76. Barrilero, R.; Ramírez, N.; Vallvé, J. C.; Taverner, D.; Fuertes, R.; Amigó, N.; Correig, X., Unravelling and Quantifying the "NMR-Invisible" Metabolites Interacting with Human Serum Albumin by Binding Competition and T2 Relaxation-Based Decomposition Analysis. *Journal of Proteome Research* **2017,** *16* (5), 1847-1856.

77. Fasano, M.; Curry, S.; Terreno, E.; Galliano, M.; Fanali, G.; Narciso, P.; Notari, S.; Ascenzi, P., The extraordinary ligand binding properties of human serum albumin. *IUBMB life* **2005,** *57* (12), 787-796.

78. Psychogios, N.; Hau, D. D.; Peng, J.; Guo, A. C.; Mandal, R.; Bouatra, S.; Sinelnikov, I.; Krishnamurthy, R.; Eisner, R.; Gautam, B.; Young, N.; Xia, J.; Knox, C.; Dong, E.; Huang, P.; Hollander, Z.; Pedersen, T. L.; Smith, S. R.; Bamforth, F.; Greiner, R.; McManus, B.; Newman, J. W.; Goodfriend, T.; Wishart, D. S., The Human Serum Metabolome. *PLOS ONE* **2011,** *6* (2), e16957.

79. Tatlidil, D.; Ucuncu, M.; Akdogan, Y., Physiological concentrations of albumin favor drug binding. *Physical Chemistry Chemical Physics* **2015,** *17* (35), 22678-22685.

80. Cousin, S. F.; Kaděrávek, P.; Bolik-Coulon, N.; Gu, Y.; Charlier, C.; Carlier, L.; Bruschweiler-Li, L.; Marquardsen, T.; Tyburn, J.-M.; Brüschweiler, R.; Ferrage, F., Time-Resolved Protein Side-Chain Motions Unraveled by High-Resolution Relaxometry and Molecular Dynamics Simulations. *J. Am. Chem. Soc.* **2018,** *140* (41), 13456-13465.

81. Akaike, H., A new look at the statistical model identification. *IEEE Transactions on Automatic Control* **1974,** *19* (6), 716-723.

82. Ferrer, M. L.; Duchowicz, R.; Carrasco, B.; de la Torre, J. G.; Acuña, A. U., The conformation of serum albumin in solution: a combined phosphorescence depolarization-hydrodynamic modeling study. *Biophysical journal* **2001,** *80* (5), 2422-2430.

83. García de la Torre, J.; Huertas, M. L.; Carrasco, B., HYDRONMR: Prediction of NMR Relaxation of Globular Proteins from Atomic-Level Structures and Hydrodynamic Calculations. *Journal of Magnetic Resonance* **2000,** *147* (1), 138-146.

84. Koenig, S. H.; Brown, R. D., Field-cycling relaxometry of protein solutions and tissue: Implications for MRI. *Progress in Nuclear Magnetic Resonance Spectroscopy* **1990,** *22* (6), 487-567.

85. Laliberté, M., Model for Calculating the Viscosity of Aqueous Solutions. *Journal of Chemical & Engineering Data* **2007,** *52* (2), 321-335.

86. Zhang, A.; Sun, H.; Wang, X., Serum metabolomics as a novel diagnostic approach for disease: a systematic review. *Anal Bioanal Chem* **2012,** *404* (4), 1239-45.

87. Takahashi, N.; Ortel, T. L.; Putnam, F. W., Single-chain structure of human ceruloplasmin: the complete amino acid sequence of the whole molecule. *Proceedings of the National Academy of Sciences* **1984,** *81* (2), 390-394.

88. Schwaeble, W.; Zwirner, J.; Schulz, T. F.; Linke, R. P.; Dierich, M. P.; Weiss, E. H., Human complement factor H: expression of an additional truncated gene product of 43 kDa in human liver. *European journal of immunology* **1987,** *17* (10), 1485-1489.

89. Refetoff, S., Inherited thyroxine-binding globulin abnormalities in man. *Endocrine Reviews* **1989,** *10* (3), 275-293.

90. Pepys, M. B.; Hirschfield, G. M., C-reactive protein: a critical update. *The Journal of clinical investigation* **2003,** *111* (12), 1805-1812.

91. Colombo, S.; Buclin, T.; Decosterd, L. In *Orosomucoid plasma concentration and genetic variants: effects on HIV protease inhibitor clearance and cellular accumulation*, 7th International Workshop on Clinical Pharmacology of HIV Therapy, 2006; pp 20-22.

92. Wobeto, V. P. d. A.; Zaccariotto, T. R.; Sonati, M. d. F., Polymorphism of human haptoglobin and its clinical importance. *Genetics and Molecular Biology* **2008,** *31* (3), 602-620.

93. Donato, L. J.; Jenkins, S. M.; Smith, C.; Katzmann, J. A.; Snyder, M. R., Reference and Interpretive Ranges for α1-Antitrypsin Quantitation by Phenotype in Adult and Pediatric Populations. *American journal of clinical pathology* **2012,** *138* (3), 398-405.

94. Soleimani, N.; Hosseinzadeh, M.; Habibagahi, Z., Value of serum glucose-6-phosphate isomerase in patients with rheumatoid arthritis and correlation with disease activity: A case-control study. *Journal of education and health promotion* **2019,** *8*, 125-130.

95. Ghini, V.; Quaglio, D.; Luchinat, C.; Turano, P., NMR for sample quality assessment in metabolomics. *New Biotechnology* **2019,** *52*, 25-34.

96. Jaseňáková, Z.; Zapletal, V.; Padrta, P.; Zachrdla, M.; Bolik-Coulon, N.; Marquardsen, T.; Tyburn, J.-M.; Žídek, L.; Ferrage, F.; Kaděrávek, P., Boosting the resolution of low-field 15N relaxation

experiments on intrinsically disordered proteins with triple-resonance NMR. *Journal of Biomolecular NMR* **2020,** *74* (2), 139-145.

97. Nicholson, J. K.; Foxall, P. J. D.; Spraul, M.; Ferrant, R. D.; Lindon, J. C., 750 MHz ^{1}H and ^{1}H-^{13}C spectroscopy of human blood plasma. *Analytical Chemistry*, **1995,** *67*, (5), 793-811.

98. Beckonert, O.; Keun, H. C.; Ebbels, T. M. D.; Bundy, J.; Holmes, E.; Lindon, J. C.; Nicholson, J. K., Metabolic profiling, metabolomic and metabonomic procedures for NMR spectroscopy of urine, plasma, serum and tissue extracts. *Nature Protocols* **2007,** *2* (11), 2692-2703.

99. McKay, R. T., How the 1D-NOESY suppresses solvent signal in metabonomics NMR spectroscopy: An examination of the pulse sequence components and evolution. *Concepts in Magnetic Resonance Part A* **2011,** *38A* (5), 197-220.

100. Piotto, M.; Saudek, V.; Sklenář, V., Gradient-tailored excitation for single-quantum NMR spectroscopy of aqueous solutions. *Journal of Biomolecular NMR* **1992,** *2* (6), 661-665.

101. Griffin, J. L.; Nicholls, A. W.; Keun, H. C.; Morthishire-Smith, R. J.; Nicholson, J. K.; Kuehn, T., Metabolic profiling of rodent biological fluids *via* ^{1}H NMR spectroscopy using a 1mm microlitre probe. *The Analyst*, **2002,** *127*, (5), 582-584.

102. Robertson, A.; Brodersen, R., Effect of lactate, pyruvate, acetone, acetoacetate, and β-hydroxybutyrate on albumin binding of bilirubin. *The Journal of pediatrics* **1983,** *102* (3), 433-438.

103. Chatham, J. C.; Forder, J. R., Lactic acid and protein interactions: implications for the NMR visibility of lactate in biological systems. *Biochimica et Biophysica Acta (BBA)-General Subjects* **1999,** *1426* (1), 177-184.

104. Nicholson, J. K.; O'Flynn, M. P.; Sadler, P. J.; Macleod, A. F.; Juul, S. M.; Sönksen, P. H., Proton-nuclear-magnetic-resonance studies of serum, plasma and urine from fasting normal and diabetic subjects. *Biochemical Journal* **1984,** *217* (2), 365-375.

105. Jupin, M.; Michiels, P. J.; Girard, F. C.; Spraul, M.; Wijmenga, S. S., NMR identification of endogenous metabolites interacting with fatted and non-fatted human serum albumin in blood plasma: Fatty acids influence the HSA–metabolite interaction. *J. Magn. Reson.* **2013,** *228*, 81-94.

106. Gowda, N. G. A.; Djukovic, D., Overview of Mass Spectrometry-Based Metabolomics: Opportunities and Challenges. Humana Press: New York, 2014.

107. Anderson, N. L.; Anderson, N. G., The human plasma proteome: history, character, and diagnostic prospects. *Molecular & cellular proteomics* **2002,** *1* (11), 845-867.

108. Gowda, N. G. A.; Gowda Y. N.; Raftery, D., Expanding the Limits of Human Blood Metabolite Quantitation Using NMR Spectroscopy. *Analytical Chemistry* **2015**, *87* (1), 706-715.

109. Gowda, N. G. A.; Raftery D., Recent Advances in NMR-Based Metabolomics. *Analytical Chemistry* **2017**, *89* (1), 490-510.

110. Bolik-Coulon, N.; Kadeřávek, P.; Pelupessy, P.; Dumez, J.-N.; Ferrage, F.; Cousin, S. F., Theoretical and computational framework for the analysis of the relaxation properties of arbitrary spin systems. Application to high-resolution relaxometry. *J. Magn. Reson.* **2020,** *313*, 106718.

111. Kadeřávek, P.; Bolik-Coulon, N.; Cousin, S. F.; Marquardsen, T.; Tyburn, J.-M.; Dumez, J.-N.; Ferrage, F., Protein Dynamics from Accurate Low-Field Site-Specific Longitudinal and Transverse Nuclear Spin Relaxation. *The Journal of Physical Chemistry Letters* **2019,** *10* (19), 5917-5922.

112. Cavanagh, J.; Fairbrother, W. J.; Palmer Iii, A. G.; Rance, M.; Skelton, N. J., In *Protein NMR Spectroscopy (Second Edition)*, Academic Press: Burlington, 2007.

113. Mayer, M.; Meyer, B., Group Epitope Mapping by Saturation Transfer Difference NMR To Identify Segments of a Ligand in Direct Contact with a Protein Receptor. *J. Am. Chem. Soc.* **2001**, *123* (25), 6108-6117.

114. Jayalakshmi, V.; Krishna, N. R., Complete Relaxation and Conformational Exchange Matrix (CORCEMA) Analysis of Intermolecular Saturation Transfer Effects in Reversibly Forming Ligand–Receptor Complexes. *J. Magn. Reson.* **2002**, *155* (1), 106-118.

115. Cousin, S. F.; Kadeřávek, P.; Bolik-Coulon, N.; Ferrage, F., Determination of Protein ps-ns Motions by High-Resolution Relaxometry. In *Protein NMR: Methods and Protocols*, Ghose, R., Ed. Springer New York: New York, NY, 2018; pp 169-203.

116. Delaglio, F.; Grzesiek, S.; Bax, A.; Vuister, G. W.; Zhu, G.; Pfeifer, J., NMRPipe: A multidimensional spectral processing system based on UNIX pipes. *Journal of Biomolecular NMR* **1995,** *6* (3), 277-293.

117. Eaton, J. W.; Bateman, D.; Hauberg, S.; Wehbring, R., GNU Octave version 4.2.0 manual: a high-level interactive language for numerical computations. **2016**.

Supporting information

Detection of Metabolite-Protein Interactions in Complex Biological Samples by High-Resolution Relaxometry: Toward Interactomics by NMR

Ziqing Wang[1], Simone Pisano[1], Veronica Ghini[2], Pavel Kadeřávek[1], Milan Zachrdla[1], Philippe Pelupessy[1], Morgan Kazmierczak[1], Thorsten Marquardsen[3], Jean-Max Tyburn[3], Guillaume Bouvignies[1], Giacomo Parigi[2,5,6], Claudio Luchinat[2,5,6*], Fabien Ferrage[1,*]

1. Laboratoire des Biomolécules, LBM, Département de chimie, École normale supérieure, PSL University, Sorbonne Université, CNRS, 75005 Paris, France

2. Consorzio Interuniversitario Risonanze Magnetiche MetalloProteine (CIRMMP), via Sacconi 6, Sesto Fiorentino, 50019 Italy

3. Bruker BioSpin GmbH; Silberstreifen 4, 76287 Rheinstetten, Germany

4 Bruker BioSpin ; 34 rue de l'Industrie BP 10002, 67166 Wissembourg Cedex, France

5. Magnetic Resonance Center (CERM), University of Florence, via Sacconi 6, Sesto Fiorentino, 50019 Italy

6. Department of Chemistry "Ugo Schiff", University of Florence, via della Lastruccia 3, Sesto Fiorentino, 50019 Italy

*luchinat@cerm.unifi.it; Fabien.Ferrage@ens.psl.eu

Table of Contents

1. Experimental setup and examples of relaxation decays

1.1 Pulse sequence

The relaxometry experiments were derived from the conventional so-called 1D NOESY pulse-sequence[1] by introducing a relaxation delay at low field after the mixing time (τ_{mix}) and before the last $\pi/2$ pulse (Fig. S1). The sample is transferred to a desired low field B_{LF} (from 0.015 to 10 T) with a transfer time 55 ms < τ_{HF-LF} < 210 ms. The sample is kept in that position for a variable relaxation delay T_{rel} and then transferred back to high field with a transfer time 60 ms < τ_{LF-HF} < 260 ms for detection. To measure relaxation rates at 14.1T, the shuttle transfers are simply omitted, such that the sample stays at high field during the whole experiment. The polarization of water can recover during the shuttle transfers and the stabilization delays τ_{st} so that it is necessary to perform an additional water suppression before detection with the WATERGATE (WG) scheme.[2] Proper suppression of the strong signal of the solvent at each scan is necessary to suppress artefacts due to residual vibrations of the sample.
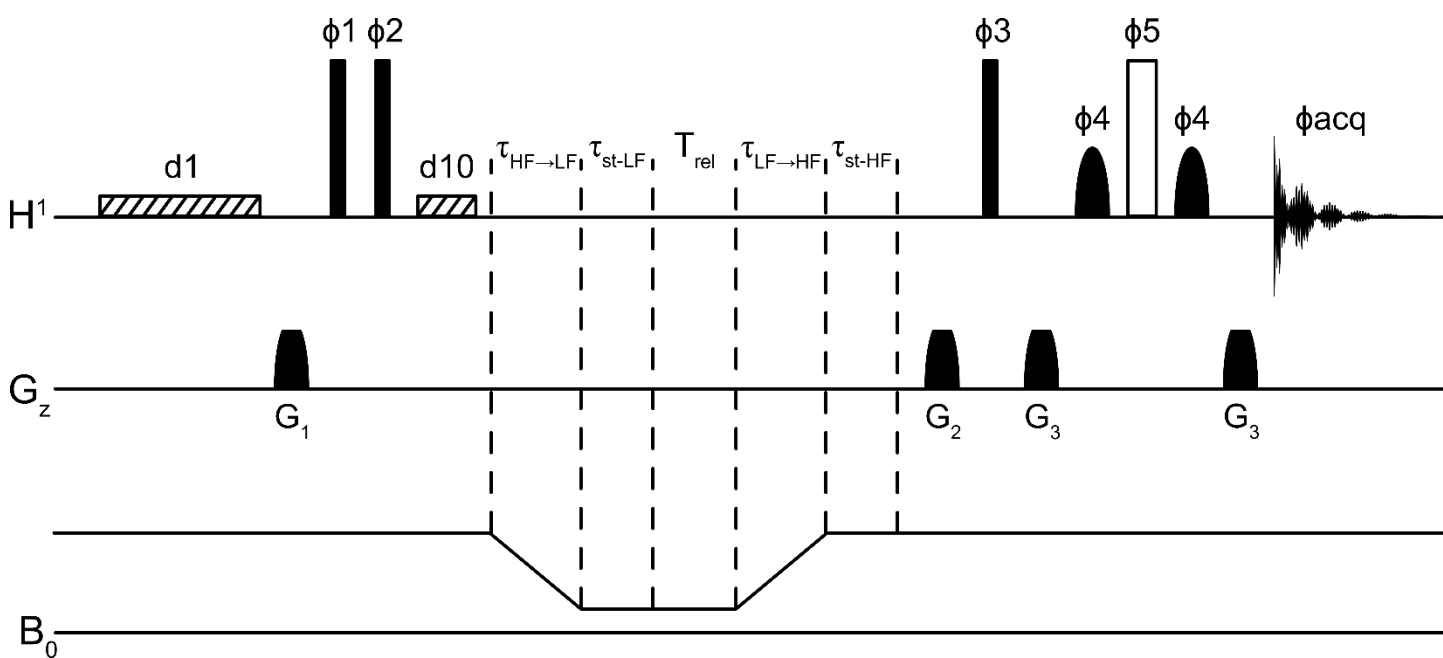

Figure S1. 1D NOESY experiment adapted for high-resolution relaxometry experiment: a relaxation delay is added after the mixing time and WATERGATE block is inserted before detection for better solvent signal suppression. 1D NOESY_WG pulse sequence used to measure relaxation dispersion profiles. The sample is moved from the high-field magnetic center of the spectrometer to a chosen position at low field and back during the period 55 ms < τ_{HF-LF} < 210 ms and 60 ms < τ_{LF-HF} < 260 ms, respectively. The variable relaxation delay at low magnetic field is labelled T_{rel}. A short stabilization delay at low field τ_{st-LF} (~10 ms) is necessary to switch the pneumatic system. The stabilization delay after the sample returns to the high-field position τ_{st-HF} is necessary before acquisition, mostly for vibration damping. For model samples τ_{st-HF} = 100 ms was sufficient, whereas for serum samples, a longer delay τ_{st-HF} = 250 ms was employed. Narrow and wide rectangles represent $\pi/2$ and π proton pulses, respectively; and the bell shapes represent 1.5 ms selective $\pi/2$ sinc-shaped pulses on the water signal. Striped rectangles stand for continuous-wave pre-saturation irradiation applied for durations τ_{sat1} = 4 s and τ_{sat2} = 10 ms with a low amplitude (75 Hz). The phase cycles were : ϕ_1=(x, -x); ϕ_2=8(x), 8(-x); ϕ_3=2(x), 2(-x), 2(y), 2(-y); ϕ_4=2(y), 2(-y), 2(-x), 2(x); ϕ_5=2(-y), 2(y), 2(x), 2(-x); ϕ_{acq}= (x, -x, -x, x, y, -y, -y, y, -x, x, x, -x, -y, y, y, -y). The maximum amplitudes of the "smoothed squared" 1 ms pulsed field gradients G_1, G_2 and G_3 applied along z-axis were 8.5, 4 and 20 G/cm, respectively.

3

1.2 Relaxation delays

The delays T_{rel} were adapted depending on the shuttling distance (*i.e.* magnetic field), and expected relaxation rates. They are reported in Table S1.

Table S1. List of relaxation delays for each relaxation position in the stray field.

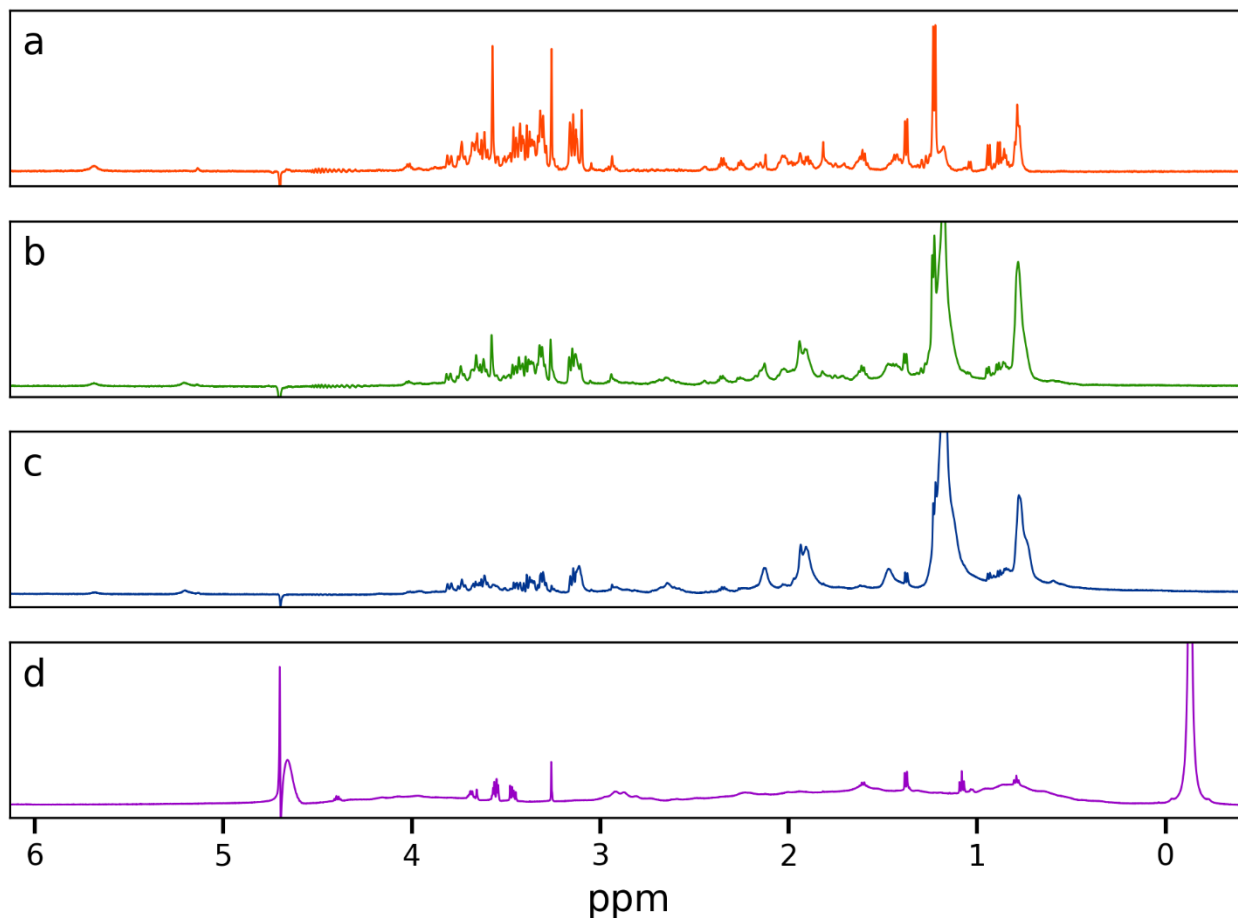| Field range (T)	List of relaxation delays (s)
14.1 – 2.5	0.001, 1, 0.1, 0.6, 0.2, 0.8, 0.4
2.5 – 0.33	0.8, 0.1, 0.5, 0.2, 0.65, 0.35, 0.001
0.33 – 0.1	0.001, 0.6, 0.05, 0.35, 0.15, 0.45, 0.25
0.1 – 0.02	0.001, 0.4, 0.05, 0.25, 0.1, 0.3, 0.15
0.02 – 0.015	0.2, 0.025, 0.1, 0.05, 0.15, 0.075, 0.001

1.3 Examples of spectral data for HRR

Figure S2. Spectra recorded with the sequence described in section 1.1. Spectra a to c are from a serum sample, spectrum d is from a model sample with 0.5 mM alanine, 50 mM TSP and 0.5 mM BSA. In order to compensate for the signal loss at lower fields, several FIDs were recorded for each T_{rel}. Hence, the actual intensity is given by the product $NS \cdot FIDs$. For each spectrum the intensity was scaled for graphical convenience. a) Relaxation field = 47 mT, NS = 16, T_{rel} = 1 ms, 200 FIDs, total number of scans: 3200. b) Relaxation field = 1.25 T, NS = 16, T_{rel} = 1 ms, 76 FIDs, total number of scans: 1216. c) Relaxation field = 14.1 T (i.e. without shuttling), NS = 16, T_{rel} = 1 ms, 19 FIDs, total number of scans: 304. d) Relaxation field = 14.1 T (i.e. without shuttling), NS = 8, T_{rel} = 1 ms, 38 FIDs, total number of scans: 304.
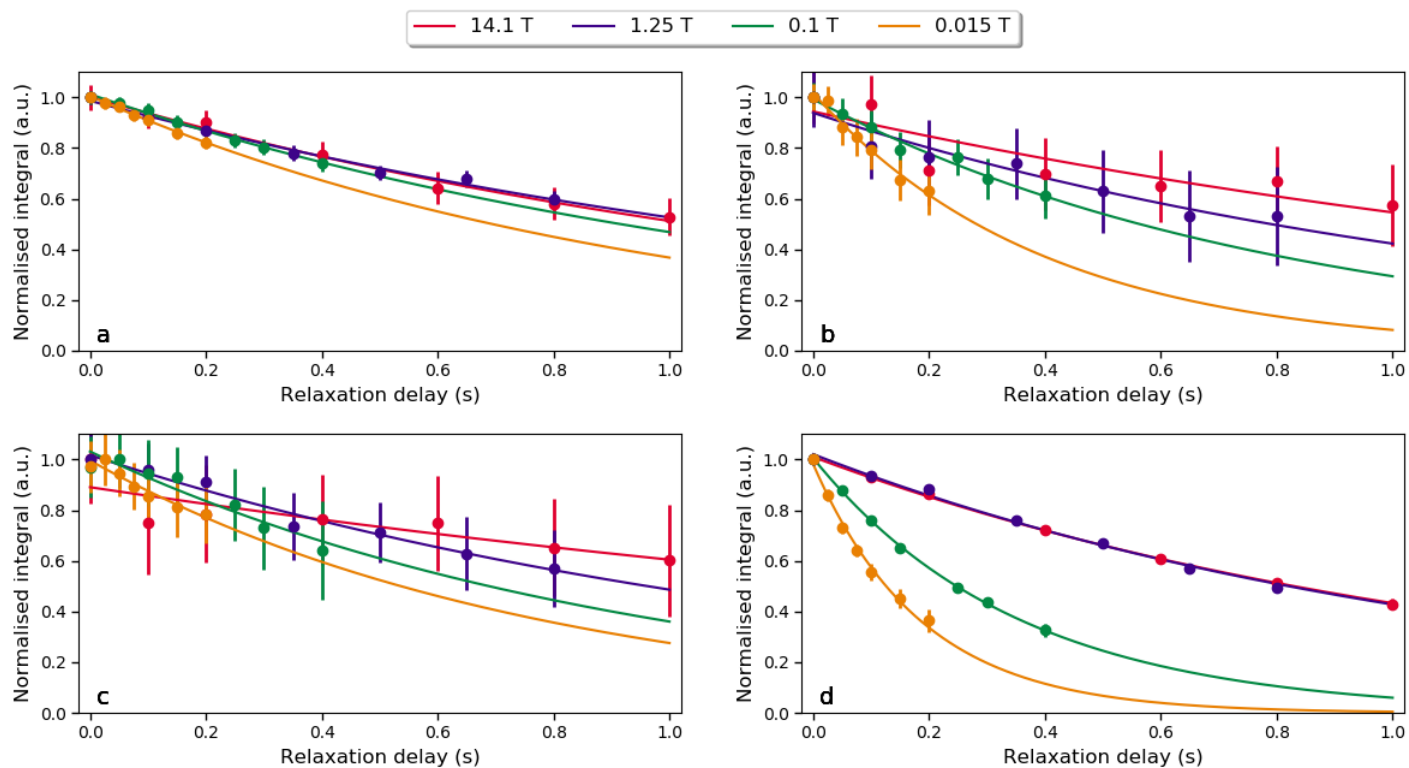
1.4 Examples of relaxation decays

Figure S3. Examples of relaxation decays of four different compounds in human blood serum at four different fields. The data was recorded with the pulse sequence described in section 1.1 and relaxation delays from Table S1. The relaxation delays correspond to those reported in section 1.2. a) Alanine. b) Creatinine. c) Glutamine. d) Lactate.

2. Proton-proton distances used in the analyses

Here, we give the intra-methyl proton-proton distances r_{HH} used for the quantitative analysis of NMRD profiles of three compounds.

Molecule	r_{HH}	Source
3-TrimethylSilyl Propionic Acid (TSP)	179 pm	https://pubchem.ncbi.nlm.nih.gov/compound/3-_Trimethylsi-lyl_propionic-acid
Alanine	175 pm	https://pubchem.ncbi.nlm.nih.gov/compound/DL-Alanine
Lactic acid/Lactate	177 pm	https://pubchem.ncbi.nlm.nih.gov/compound/Lactic-acid

3. Fitting models for NMRD profiles of TSP in the model sample

In all models, the rotation of the trimethylsilyl group is considered possible in the free form and hindered in the bound form with an order parameter imposed by geometry.

<u>3.1 Model M1: model adopted as most reliable</u>

Model 1 is the simplest model of spectral density function (see Equations 1-4), with only dipolar contributions from non-methyl protons in the bound state, a small population of the bound form: $p_B << 1$, and infinitely fast rotation of the TMS group in the free form. Model 1 is the model used in the data analysis given in Figure 3. It is the best fitting model based on the Akaike information criterion (see Table S2).

$$R_1 = A_B p_B [J(0, \tau_c^B) + 3J(\omega, \tau_c^B) + 6J(2\omega, \tau_c^B)] + S_{TMS}^2 A_{methyl} [J(\omega, \tau_c^F) + 4J(2\omega, \tau_c^F)]$$

$$[S1]$$

where, p_B is the population of the bound form, τ_c^B and τ_c^F are the correlation times of the bound and free states, respectively. $A_B = S^2 \frac{1}{64} \frac{\mu_0^2 \gamma_H^4 \hbar^2}{\pi^2 r_{env}^6}$ is the amplitude of dipolar interaction with the environment, scaled by the order parameter due to infinitely fast methyl group rotation $S^2 = ¼$, μ_0 is the permeability of vacuum, γ_H is the proton gyromagnetic ratio, r_{env} is the effective proton-proton distance. $A_{methyl} = S^2 \frac{3}{32} \frac{\mu_0^2 \gamma^4 \hbar^2}{\pi^2 r_{HH}^6}$ is the dipolar interaction amplitude inside the methyl group, calculated based on the distance between two protons inside the methyl group (r_{HH} = 179 pm), scaled by the order parameter due to infinitely fast methyl group rotation $S^2 = ¼$. Moreover, the contribution for the free form accounts for the rotation of the TMS group, also considered to be infinitely fast, so that the constant A_{methyl} is multiplied by the order parameter $S_{TMS}^2 = ¼$.
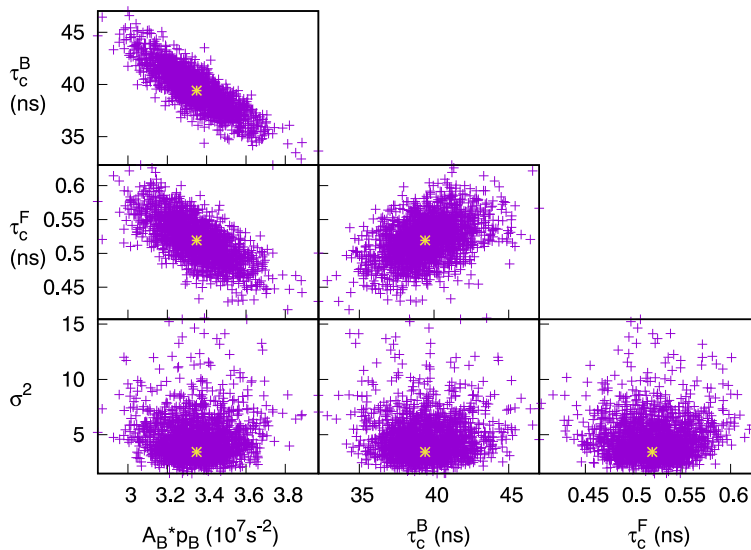

Figure S4. Plot of correlations between the 3 parameters fitted in model M1 and the variances.

3.2 Model M2:

Model 2 is similar to model 1. Model 2 includes as a parameter the correlation time for TMS rotation in the free form. We assumed that p_B is very small, so that $1 - p_B \approx 1$. The intra-methyl dipolar interaction is neglected in the bound form. In this way, the product $A_B p_B$ is a single free parameter.

$$R_1 = A_B p_B [J(0, \tau_c^B) + 3J(\omega, \tau_c^B) + 6J(2\omega, \tau_c^B)] + A_{methyl} \left\{ S_{TMS}^2 [J(\omega, \tau_c^F) + 4J(2\omega, \tau_c^F)] + (1 - S_{TMS}^2) \left[J\left(\omega, \frac{\tau_c^F \tau_c^{TMS}}{\tau_c^F + \tau_c^{TMS}}\right) + 4J\left(2\omega, \frac{\tau_c^F \tau_c^{TMS}}{\tau_c^F + \tau_c^{TMS}}\right) \right] \right\}.$$
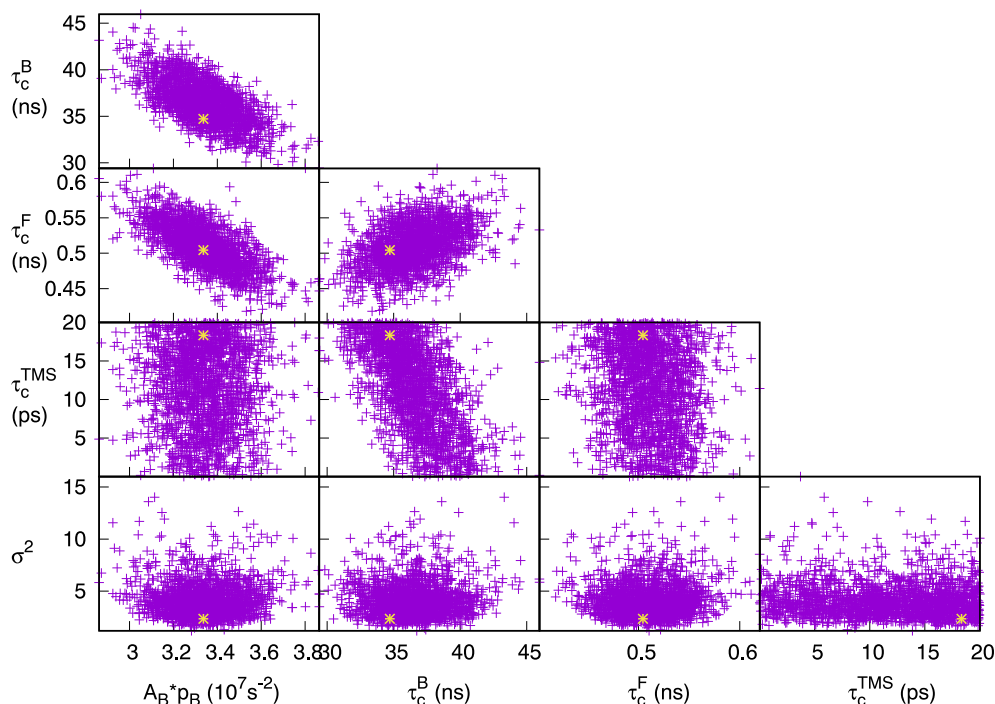
$$[S2]$$

Figure S5. Plot of correlations between 4 parameters fitted in model M2 and the calculated variances.

9

3.3 Model M3:

Here, we assume that the rotation of the TMS group is infinitely fast in the free form but we do not assume that p_B is very small. Hence, we include the contribution of intra-methyl dipole-dipole interactions in the bound form:

$$R_1 = p_B\{A_B[J(0,\tau_c^B) + 3J(\omega,\tau_c^B) + 6J(2\omega,\tau_c^B)] + A_{methyl}[J(\omega,\tau_c^B) + 4J(2\omega,\tau_c^B)]\} + (1 - p_B)A_{methyl}S_{TMS}^2[J(\omega,\tau_c^F) + 4J(2\omega,\tau_c^F)].$$ [S3]
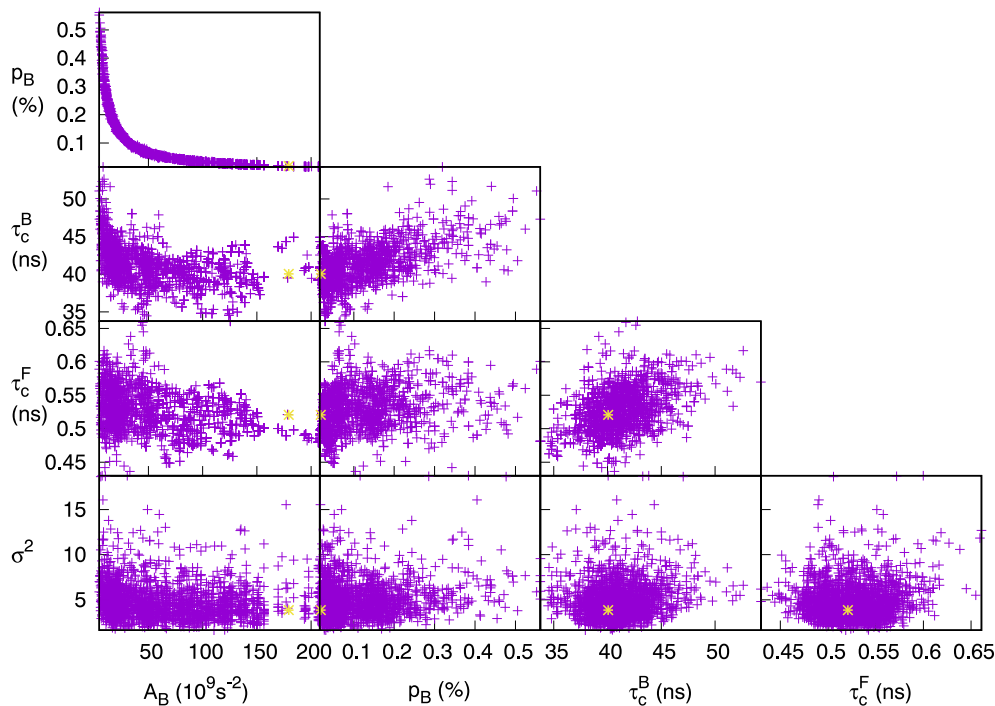

Figure S6. Plot of correlations between 4 parameters fitted in model M4 and the variances.

The strong correlation between A_B and p_B indicates that the approximations of models 1 and 2, which consist of considering only the product $A_B p_B$, are justified.

10

3.4 Model M4:

In this model, we considered the contributions of intermolecular dipolar interaction in the free and bound states (as in Model M3), and dipolar interaction with the proton environment in the bound form. The rotation of methyl group is infinitely fast in the free and bound forms, while the rotation of the TMS with a correlation time τ_c^{TMS} (as in Model M2) in the free form is hindered in the bound form. The longitudinal relaxation rate is:

$$R_1 = p_B\{A_B[J(0,\tau_c^B) + 3J(\omega,\tau_c^B) + 6J(2\omega,\tau_c^B)] + A_{methyl}[J(\omega,\tau_c^B) + 4J(2\omega,\tau_c^B)]\} + (1 - p_B)A_{methyl}\{S_{TMS}^2[J(\omega,\tau_c^F) + 4J(2\omega,\tau_c^F)] + (1 - S_{TMS}^2)\left[J\left(\omega,\frac{\tau_c^F\tau_c^{TMS}}{\tau_c^F+\tau_c^{TMS}}\right) + 4J\left(2\omega,\frac{\tau_c^F\tau_c^{TMS}}{\tau_c^F+\tau_c^{TMS}}\right)\right]\},$$
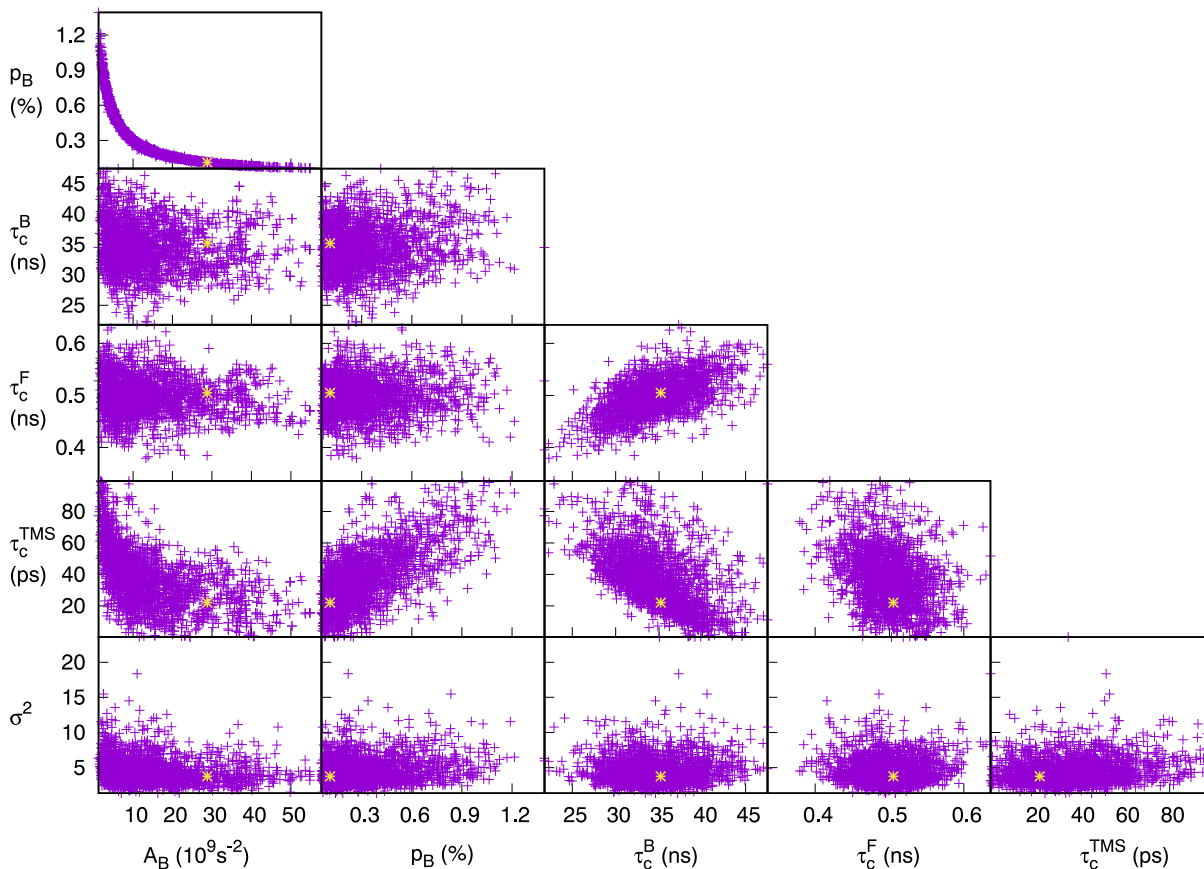
$$[S4]$$

Figure S7. Plot of correlations between 5 parameters fitted in model M2 and the calculated variances.

Again, the correlation between parameters A_B and p_B indicates that the approximations of models 1 and 2, which consist of considering only the product $A_B p_B$, are justified.

4. Comparison of models by their corrected Akaike information criteria (AICc)

The relative probabilities of models M1-M4 were compared based on the corrected Akaike Information Criteria. The AICc for model Mi is noted $AICc_i$:[3]

$$AICc_i = n \times log\left(\frac{\chi^2}{n}\right) + \frac{2k_i n}{n - k_i - 1}$$

where n = 19 is the number of experimental data, here relaxation rates, and k_i is the number of parameters in the fitting model M1: $k_1 = 3$; $k_2 = k_3 = 4$; and $k_4 = 5$. The fit of the NMRD profiles and the calculated parameters using different models are summed up in Table S2. The lowest AICc value is $AICc_1$, obtained for fitting model M1, indicating that M1 is the most probable model. This model is used for data analysis in the model sample and in serum.

Table S2. Comparison of fitting results the variance σ^2 and χ^2 obtained from different models. The quality of the models is compared with AIC.

	Number of parameters	$A_B p_B$ (10^9 s^{-2})	τ_c^B (ns)	τ_c^F (ns)	τ_c^{TMS} (ps)	σ^2	χ^2	$AICc_i$
M1	3	0.034 ± 0.0016	39.4 ± 1.9	0.52 ± 0.03	-	3.45	63.92	17.6
M2	4	0.034 ± 0.0016	34.7 ± 2.3	0.50 ± 0.03	18 ± 6	2.33	56.15	19.8
M3	4	A = 179 ± 52 p_B = 0.018 ± 0.076 % $\overline{0.032 ± 0.0012}$	40.1 ± 2.2	0.52± 0.03	-	3.86	65.01	21.0
M4	5	A = 28.8 ± 10.5 p_B = 0.11 ± 0.22 % $\overline{0.033 ± 0.0033}$	35.2 ± 4.0	0.51± 0.04	22 ± 18	4.31	56.80	23.7

Equation S1 was adapted to fit the NMRD profile of methyl protons of alanine ([Equation S5]) and lactate ([Equation S6]). No interaction was detected for alanine, the expression of R$_1$ is then, with a single free parameter τ_c^F:

$$R_1 = A_{methyl}[J(\omega, \tau_c^F) + 4J(2\omega, \tau_c^F)], \qquad \text{[S5]}$$

with $A_{methyl} = 7.44 \times 10^9 s^{-2}$.

The model used to analyze the NMR profile of the methyl group of lactate is adapted from model 1, where the only internal motion considered is the infinitely fast rotation of the methyl group.

$$R_1 = A_B p_B[J(0, \tau_c^B) + 3J(\omega, \tau_c^B) + 6J(2\omega, \tau_c^B)] + A_{methyl}[J(\omega, \tau_c^F) + 4J(2\omega, \tau_c^F)], \qquad \text{[S6]}$$

with $A_{methyl} = 6.95 \times 10^9 s^{-2}$.

5. Size distribution of macromolecules in serum

The water FFC NMRD profiles of three serum samples were fitted with 4 correlation times. The equation used for the fit was:

$$R_1 = A + B \sum_i^4 p_i \left[0.2J(\omega, \tau_c^i) + 0.8J(2\omega, \tau_c^i)\right], \qquad \text{[S7]}$$

where A accounts both for the relaxation contributions from protons with correlation times faster than 10^{-9} s and for non-dispersive contributions, in addition to the relaxation rate of the pure solvent in the absence of macromolecules, B is the dipolar interaction amplitude with the macromolecules and p_i is the population fraction of macromolecules with effective correlation time τ_c^i.

Table S3. Results of water relaxation in serum samples from 3 different donors with Equation S7.

Parameter	Donor 1		Donor 2		Donor 3	
Temperature (°C)	25	37	25	37	25	37
A (s^{-1})	0.59 ± 0.02	0.48 ± 0.02	0.58 ± 0.01	0.48 ± 0.01	0.59 ± 0.01	0.48 ± 0.01
B (10^6 s^{-2})	82 ± 8		71 ± 2		75 ± 3	
p_1	0.005 ± 0.001		0.0032 ± 0.0004		0.0039 ± 0.0004	
τ_c^1 (µs)	1.5 ± 0.1	1.3± 0.1	1.0 ± 0.1	1.7 ± 0.1	1.7 ± 0.1	1.5 ± 0.1
p_2	0.04 ± 0.01		0.031 ± 0.002		0.042 ± 0.004	
τ_c^2 (ns)	220 ± 40	170 ± 30	360 ± 30	280 ± 20	270 ± 20	210 ± 20
p_3	0.39 ± 0.04		0.31 ± 0.01		0.31 ± 0.01	
τ_c^3 (ns)	38 ± 4	32 ± 3	51 ± 3	42 ± 2	49 ± 3	40 ± 2
p_4	0.56 ± 0.041		0.66 ± 0.010		0.64 ± 0.011	
τ_c^4 (ns)	5.9 ± 2	8.5 ± 2	9.1 ± 0.8	8.5 ± 0.7	8.3 ± 0.8	8.4 ± 0.7

6. Measurement of transverse relaxation rate R_2 of creatinine methyl protons

The experiments for measuring the transverse relaxation rate R_2 of methyl protons in creatinine were performed on two samples of 0.8 mM creatinine with and without 0.5 mM bovine serum albumin (BSA), respectively. The solvent was a phosphate buffer at pH 7.4 with 35 mM Na_2HPO_4 and 0.58 mM NaN_3 in H_2O/D_2O 90/10 (v/v). The experiments were repeated 5 times and the results are reported in Table S4. Relaxation rates were fitted with a simple home-built Python script. The pulse sequence used is shown in Figure S8.

Table S4. Results on the measurement of R_2 of creatinine methyl protons with and without BSA.

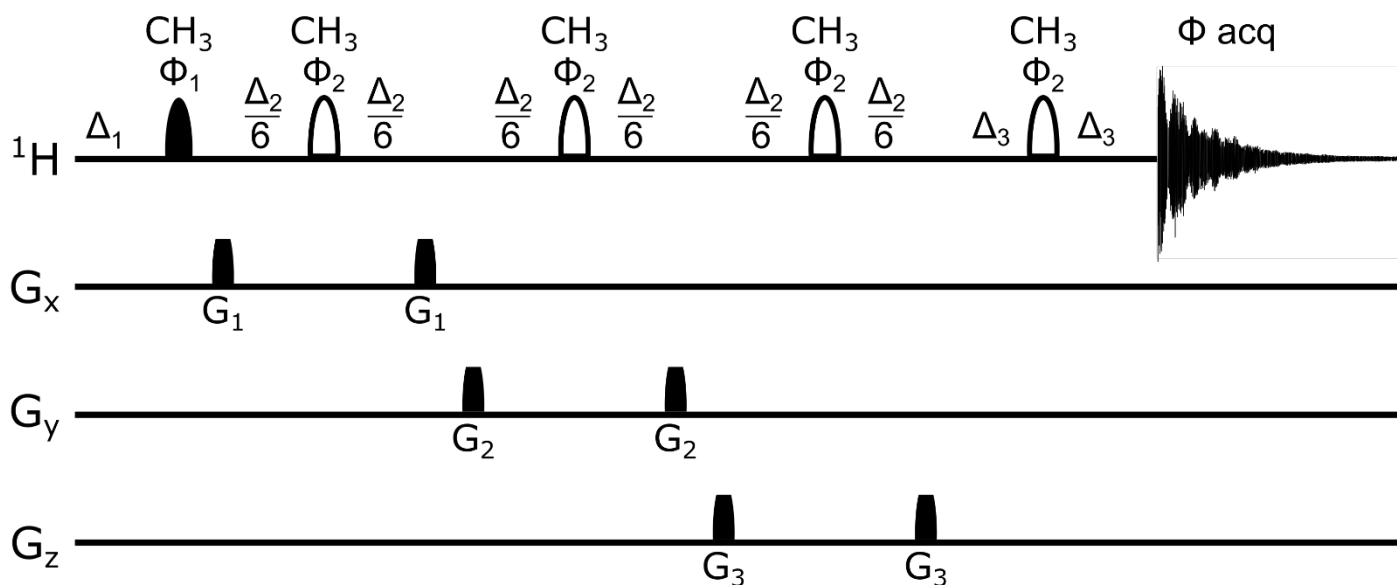|	R_2 (s^{-1}) exp. 1	R_2 (s^{-1}) exp. 2	R_2 (s^{-1}) exp. 3	R_2 (s^{-1}) exp. 4	R_2 (s^{-1}) exp. 5	Average
Creatinine without BSA	2.49 ± 0.02	2.52 ± 0.02	2.49 ± 0.02	2.48 ± 0.02	2.50 ± 0.03	2.50 ± 0.01
Creatinine with BSA	21.94 ± 0.09	21.77 ± 0.06	21.92 ± 0.09	21.80 ± 0.06	21.87 ± 0.12	21.86 ± 0.03

Figure S8. Experiment designed for measuring transverse relaxation rates in our model samples. Filled and open bell- shapes represent selective $\pi/2$ and π shaped pulses, respectively. Initially a 2 ms sinc-shaped $\pi/2$ pulse is applied on the desired methyl signal. The following spin-echo sequence was divided in three parts in order to limit the evolution of unwanted coherences. Each echo had a duration of a third of the listed delay Δ_2. At the center of each echo a Q3 shaped-pulse on the wanted methyl signal (8 ms) was applied in order to refocus the homonuclear scalar coupling. Finally, another echo with a fixed length was used to remove signals arising from BSA which were overlapping with the creatinine methyl signal. $\Delta_1 = 4$ s; $\Delta_2 =$ listed delay; $\Delta_3 = 20$ ms. The phase cycles were: $\phi_1 = $ (-x, -y, x, y); $\phi_2 = $ (y, -x, -y, x, -y, x, y, -x); $\phi_{acq} = $ (x, y, -x, -y). The amplitudes of the "smoothed squared" 1 ms pulsed field gradients G_1, G_2 and G_3 applied along the z-axis were 6.6, 23 and 17 G.cm^{-1}, respectively.

7. Correlation between molecular weight and correlation time estimated by HYDRONMR

In order to estimate the correlation time of a part of the proteins present in human serum, we used HYDRONMR to obtain a simple relationship between rotational correlation time and molecular weight (Fig. S9). The points in the plot represent proteins with molecular weight and crystal structure which are well defined and reported, see Table S5 for details. The reported correlation time is the average given by HYDRONMR, the estimated error is 8%.[4]
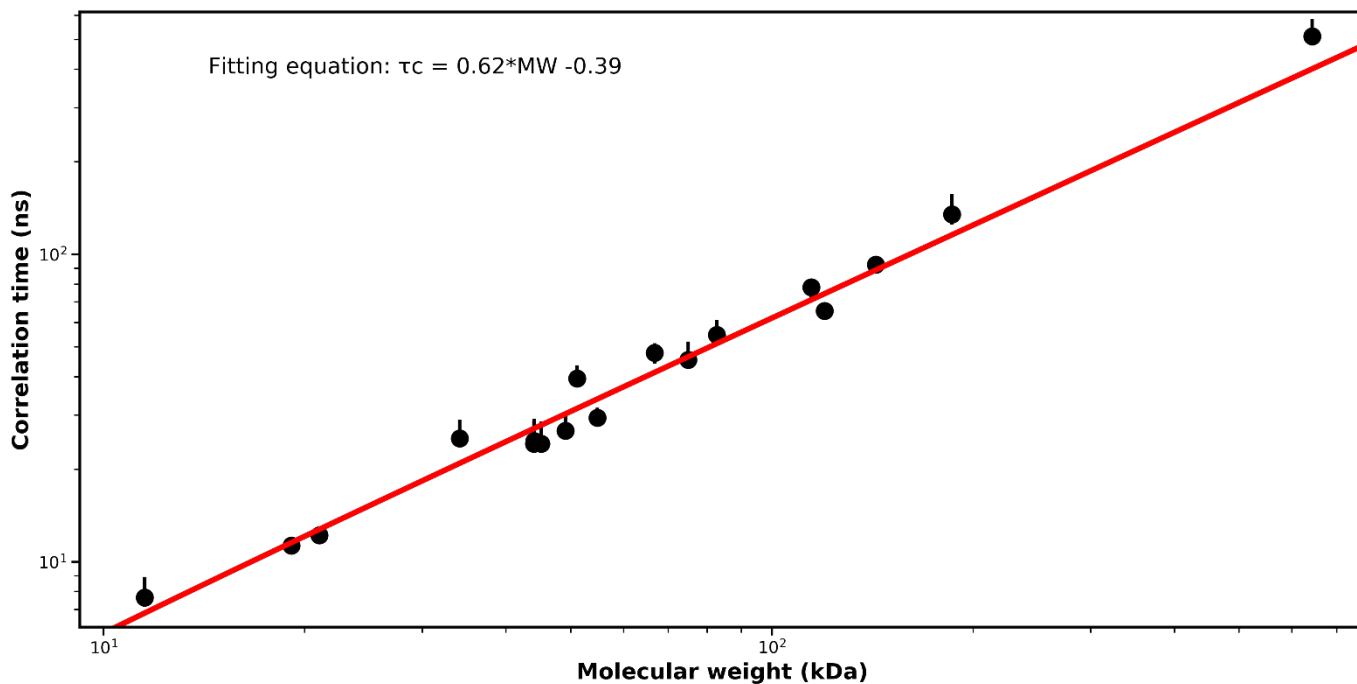

Figure S9. Plot of the correlation between molecular weight and correlation time calculated by HYDRONMR. The red fitting line has the reported empiric equation.

The empirical equation that we obtained is:

$$\frac{\tau_c}{1\ ns} = 0.62\ \frac{MW}{1\ kDa} - 0.39, \qquad [S8]$$

where τ_c is the rotational correlation time and MW is the molecular weight.

In order to assess the range of variation of an effective correlation time τ_{eff} given by HYDRONMR, we used a simple Python script to calculate the global maximum and global minimum of the spectral density function $J(\tau,\omega=0)$, derived from the correlation function for a rigid body anisotropic reorientation[5,6]:

$$J(\omega = 0) = \frac{2\tau_{eff}}{5} = \frac{A_1\tau_1 + A_2\tau_2 + A_3\tau_3 + A_4\tau_4 + A_5\tau_5}{2} \qquad [S9]$$

where:

$$A_1 = 6m^2n^2$$

$$A_2 = 6l^2n^2$$

$$A_3 = 6l^2m^2$$

15

$$A_4 = d - e$$

$$A_5 = d + e$$

where:

$$d = \frac{3(l^4 + m^4 + n^4) - 1}{2}$$

$$e = \frac{\delta_x(3l^4 + 6m^2n^2 - 1) + \delta_y(3m^4 + 6l^2n^2 - 1) + \delta_z(3n^4 + 6l^2m^2 - 1)}{6}$$

where:

$$\delta_i = \frac{D_i - D}{\sqrt{D^2 - L^2}}$$

D is a third of the trace of the diffusion tensor:

$$D = \frac{D_x + D_y + D_z}{3}$$

and:

$$L^2 = \frac{D_xD_y + D_xD_z + D_yD_z}{3}$$

The correlation times are defined as follows:

$$\tau_1 = \frac{1}{4D_x + D_y + D_z}$$

$$\tau_2 = \frac{1}{4D_y + D_x + D_z}$$

$$\tau_3 = \frac{1}{4D_z + D_x + D_y}$$

$$\tau_4 = \frac{1}{6\left(D + \sqrt{D^2 - L^2}\right)}$$

$$\tau_5 = \frac{1}{6\left(D - \sqrt{D^2 - L^2}\right)}$$

The diffusion tensor eigenvalues were obtained from HYDRONMR.
The span of the variability of the correlation time due to anisotropy for each protein is reported in Figure S9 as error bars.

8. Proteins in human serum

Table S5. List of the most concentrated proteins present in human serum. Rotational correlation times reported in black were calculated with HYDRONMR, correlation times reported in blue were calculated with Eq. S8

Protein	Concentration	MW (kDa)	No. aa	PDB code	Diff. vector eigenvalues	Correlation time (ns)
Human serum albumin[7, a]	5.3-7.6 · 10^{-4} M 35-50 g/L	66.8	585	1E7C	Dz 2.887E+06 Dy 3.617E+06 Dx 3.967E+06	47.80
Immunoglobulin G[7, b, d]	3.8-12 · 10^{-5} M 5.7-18 g/L	150				93.62
Apolipoprotein A-I[7, f, l]	3.4-5.2 · 10^{-5} M 1.0-1.5 g/L	56.1	484	3K2S		34.39
Serotransferrin[7, a]	2.8-5.2 · 10^{-5} M 2.2–4.0 g/L	74.9	660	3QYT	Dz 4.605E+06 Dy 3.053E+06 Dx 3.357E+06	45.40
α_1-Antitrypsin[8, e, m]	1.8-5.0 · 10^{-5} M 1.5-2.7 g/L	52 (44.1)	394	1QLP		31.85 (24.20)
Apolipoprotein A-II[7, c, d, l]	1.8-2.9 · 10^{-5} M 0.3-0.5 g/L	8.67	77			4.99
α_1-Acid glycoprotein[9, d, e]	1.4-2.9 · 10^{-5} M 0.6-1.2 g/L	42	183			25.65
Apolipoprotein C-III[7, c, l]	1.4 · 10^{-5} M 0.12 g/L	8.7	79	2JQ3		5.00
Vitamin D binding protein[7, a, l]	8.9-9.8 · 10^{-6} M 0.5-0.55 g/L	51.1	458	1KW2	Dz 5.003E+06 Dy 3.682E+06 Dx 3.973E+06	39.50
α_1-Antichymotrypsin[7, e, l, m]	6.1-8.1 · 10^{-6} M 0.42-0.56 g/L	69 (45.2)	400	3DLW		42.39 (24.2)
C3 complement[7, j]	5.9-9.2 · 10^{-6} M 1.1-1.7 g/L	184.6	1641	2A73		114.05
Apolipoprotein C-II[7, c, l]	4.5 · 10^{-6} M 40 mg/L	8.9	79	1SOH		5.12
Transthyretin[7, a]	3.6-7.3 · 10^{-6} M 0.2-0.4 g/L	54.8	508	1ICT	Dz 6.483E+06 Dy 5.046E+06 Dx 5.473E+06	29.40
Antithrombin III[7, e, l, m]	3.4-4.0 · 10^{-6} M 0.22-0.26 g/L	65 (49.1)	432	2B4X		39.91 (26.70)
Apolipoprotein A-IV[7, c, l]	3.4 · 10^{-6} M 0.15 g/L	43.2	376	3S84		26.39
C1 inhibitor[10, e]	3.3 · 10^{-6} M 0.25 g/L	76	478			46.73
Apolipoprotein D[7, a, l]	3.2 · 10^{-6} M 60 mg/L	19.1	169	2HZR	Dz 1.630E+07 Dy 1.399E+07 Dx 1.410E+07	11.30
Inter-α-trypsin inhibitor[7, h, l]	3.1 · 10^{-6} M 0.5 g/L	160				98.81
Factor H[7,11, d, e]	2.7-4.8 · 10^{-6} M 0.41-0.72 g/L	150	1213			92.61
α_2-Macroglobulin[7, e, m]	2.6-4.6 10^{-6} M	720	5804	4ACQ		446.01

	1.9-3.3 g/L	(643.1)				(512)
Immunoglobulin A[7, b, d]	2.5-22 · 10⁻⁶ M 0.4-3.5 g/L	160				98.81
Complement factor B[7, a]	2.1 · 10⁻⁶ M 0.2 g/L	82.8	739	2OK5	Dz 3.689E+06 Dy 2.724E+06 Dx 2.732E+06	54.70
Serum amyloid A[12, a]	1.7-4.2 · 10⁻⁶ M <5mg/L	11.5	104	4IP8	Dz 2.784E+07 Dy 1.796E+07 Dx 1.944E+07	7.66
Retinol binding protein[7, a]	1.7-4.3 · 10⁻⁶ M 35-90 mg/L	21.0	183	1JYD	Dz 1.449E+07 Dy 1.277E+07 Dx 1.362E+07	12.20
C4 complement[7, b, d]	1.7-2.9 · 10⁻⁶ M 0.35-0.6 g/L	204				126.09
Ceruloplasmin[7,13, a, m]	1.5-3.0 · 10⁻⁶ M 0.2-0.4 g/L	134 (119.9)	1046	4ENZ		82.70 (65.50)
C6 complement[7, f]	1.4-1.9 · 10⁻⁶ M 0.18-0.24 g/L	125	913	3T5O		77.11
Apolipoprotein B-100[7, d, e, l]	1.3-1.8 · 10⁻⁶ M 0.7-1.0 g/L	550.0	4540			317.69
Apolipoprotein C-I[7, c, l]	1.1· 10⁻⁶ M 70 mg/L	6.5	57	1IOJ		3.62
Haptoglobin[14, g, n]	1.0-4.5 · 10⁻⁶ M 0.5-2.2 g/L	86-900				
C9 complement[7, k]	0.5-1.4 · 10⁻⁶ M 33-95 mg/L	60.9	538	6DLW		37.36
Apolipoprotein E[7, a, l]	8.8-21 · 10⁻⁷ M 30-70 mg/L	34.1	299	2L7B	Dz 8.330E+06 Dy 5.673E+06 Dx 5.836E+06	25.20
Immunoglobulin M[7, b, d]	5.2-31 · 10⁻⁷ M 0.5-3.0 g/L	970				601.01
Apolipoprotein J[15, d, l]	4.4-13.5 · 10⁻⁷ M 35-105 mg/L	50.1	427			30.66
Complement component 1r[7, d]	4.1-5.8 · 10⁻⁷ M 34-48 mg/L	78.2	688			48.11
Complement component 1s[7, d]	4.0 · 10⁻⁷ M 34 mg/L	74.8	673			46.00
C8 complement[7, a]	3.3-7.1 · 10⁻⁷ M 49-106 mg/L	143.1	1273	3OJY	Dz 1.927E+06 Dy 1.693E+06 Dx 1.772E+06	92.70
Thyroxine binding globulin[16, e, m]	3.0 · 10⁻⁷ M 16 mg/L	54 (44.1)	395	4X30		33.09 (24.70)
C5 complement[7, a]	2.8-5.8 · 10⁻⁷ M 55-113 mg/L	186.0	1658	3CU7	Dz 1.570E+06 Dy 1.008E+06 Dx 1.121E+06	135.00
Complement factor I[7, d, e]	2.8-5.6 · 10⁻⁷ M 25-50 mg/L	88	565			54.17
C2 complement [7, d, e]	2.3 · 10⁻⁷ M 25 mg/L	110	732			67.81
C7 complement[7, e, k]	2.2-6.2 · 10⁻⁷ M	120	821			74.01

	27-74 mg/L					
Apolipoprotein B-48[7, i, l]	2.1 · 10⁻⁷ M 50 mg/L	236.7	2152			146.38
C1q complement[7, b, d]	1.8-2.7 · 10⁻⁷ M 83-125 mg/L	460				284.81
Apolipoprotein (a) [7, d, l]	1.8 · 10⁻⁷ M 0.1 g/L	498.91	4510			308.93
C-reactive protein[17, a]	6.9 · 10⁻⁹ M 0.8 mg/L	114.6	1025	3L2Y	Dz 1.772E+06 Dy 2.293E+06 Dx 2.340E+06	78.10

[a] Correlation time estimated with HYDRONMR. [b] Entry not present in UniProt, correlation time was calculated with Eq. S8. [c] Lacking tertiary folding, correlation time could not be estimated with HYDRONMR. It was instead calculated with Eq. S8. [d] Full crystal structure not reported, the correlation time was calculated with Eq. S8. [e] The molecular weight is higher that what is expected from the number of residues due to glycosylation. The mass of the glycosylated protein was used to calculate the correlation time with Eq. S8. [f] Multidomain and/or loosely connected, very flexible. The correlation time could not be estimated with HYDRONMR, it was instead calculated with Eq. S8. [g] Highly variable polymorphism, where the molecular weight can change of up to one order of magnitude. [h] It is composed by 3 heavy chain chosen between 4 different types, and one light chain chosen between two different types. [i] Molecular weight estimated from the number of residues. [j] Anisotropy is too high for estimating the correlation time with HYDRONMR, Eq. S8 was used instead. [k] Reported as part of a complex, the correlation time of the single component was calculated with Eq. S8. [l] Concentration in plasma. [m] The crystal structure of the non-glycosylated protein was used as part of the data for Fig. S9. The molecular weight of the bare peptide chain(s) and the correspondent correlation time are reported in brackets. [n] Not reported in Fig. S10.
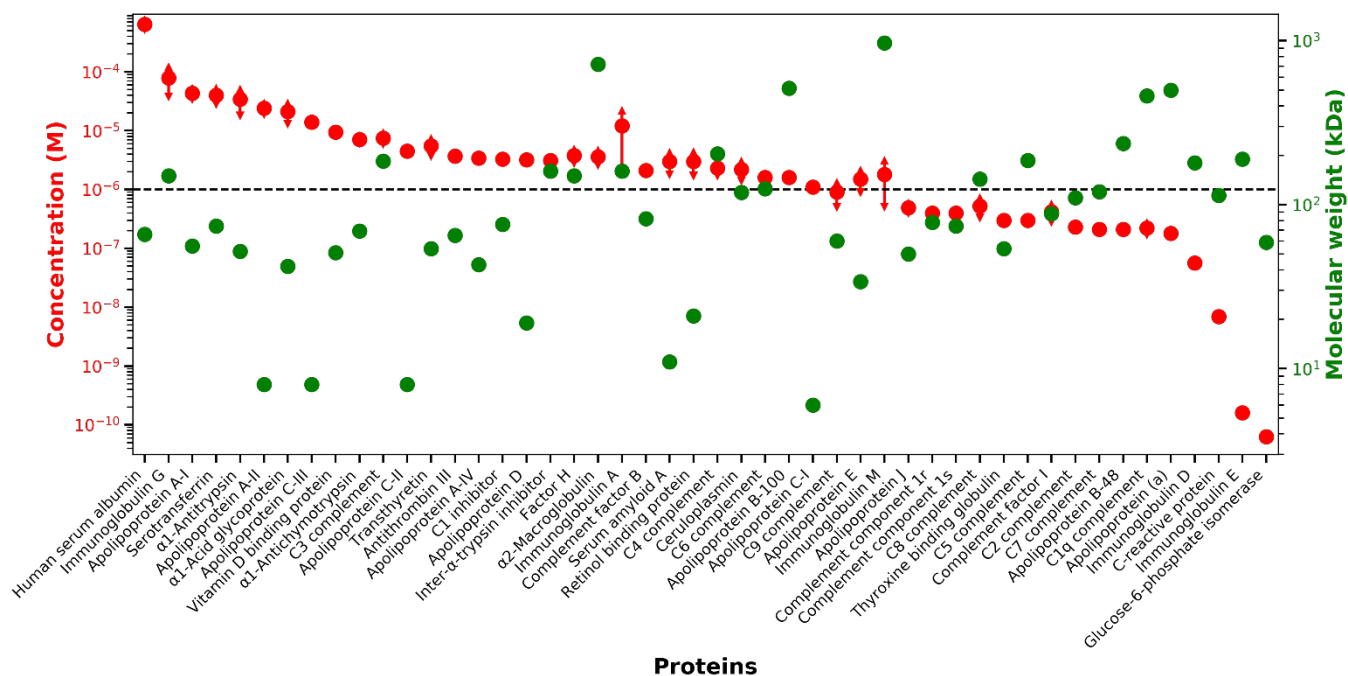

Figure S10. Representation of the molecular weight (green) and concentration (red) of the most concentrated proteins in human serum. The dashed line corresponds to the estimate of the detection limit with our current setup. The arrows represent the variability of concentration in a healthy subject.

9. Estimation of diffusion tensor and rotational correlation time with HYDRONMR

HYDRONMR Version 7.C

J. García de la Torre, M.L. Huertas and B. Carrasco, "HYDRONMR: prediction of NMR relaxation of globular proteins from atomic-level structures and hydrodynamic calculations"
J. Magnetic Reson. 147, 138-146 (2000).

Bovine serum albumin

Temperature: 298.0 K
Solvent viscosity: 0.00890 poise
Radius of atomic elements: 3.2 Angs
Translational diffusion coefficient: 6.905E-07 cm2/s

Center of diffusion (x): 4.564E-07 cm
Center of diffusion (y): 3.249E-07 cm
Center of diffusion (z): 4.510E-07 cm

Generalized (6x6) diffusion matrix: (Dtt Dtr)
                                    (Drt Drr)

7.132E-07 -2.253E-09 2.089E-09   -5.312E-03 -1.763E-03 1.118E-02
-2.240E-09 6.722E-07 -1.545E-08   -1.776E-03 8.343E-03 -2.918E-03
2.075E-09 -1.544E-08 6.862E-07   1.124E-02 -2.864E-03 -3.820E-03

-5.312E-03 -1.776E-03 1.124E-02   4.202E+06 -1.297E+05 1.098E+05
-1.763E-03 8.343E-03 -2.864E-03   -1.298E+05 3.305E+06 -1.695E+05
1.118E-02 -2.918E-03 -3.820E-03   1.098E+05 -1.695E+05 3.738E+06

ROTATIONAL DIFFUSION TENSOR
4.202E+06 -1.297E+05 1.098E+05
-1.298E+05 3.305E+06 -1.695E+05
1.098E+05 -1.695E+05 3.738E+06

Anisotropic rotational diffusion
     Eigenvalue (s^-1)   -- Eigenvector ------------
1   3.239E+06   0.0933 0.9488 0.3018
2   3.750E+06   -0.2985 -0.2625 0.9176
3   4.256E+06   0.9498 -0.1757 0.2587

Anisotropic rotational diffusion
       Dx,Dy,Dz (s^-1)   -- Eigenvector ------------
Dz   3.239E+06   0.0933 0.9488 0.3018

Dy   3.750E+06   -0.2985 -0.2625 0.9176
Dx   4.256E+06   0.9498 -0.1757 0.2587

Rotational diffusion coefficient: 3.748E+06 s-1
Rotational diffusion anisotropy: 8.809E+05 s-1
Relaxation time (1): 4.824E-08 s
Relaxation time (2): 4.771E-08 s
Relaxation time (3): 4.445E-08 s
Relaxation time (4): 4.165E-08 s
Relaxation time (5): 4.123E-08 s
Harm. mean relax.(correlation) time: 4.446E-08 s

Human serum albumin

Temperature: 298.0 K
Solvent viscosity: 0.00890 poise
Radius of atomic elements: 3.2 Angs
Translational diffusion coefficient: 6.774E-07 cm2/s

Center of diffusion (x): 4.184E-07 cm
Center of diffusion (y): 2.717E-07 cm
Center of diffusion (z): 4.836E-07 cm

Generalized (6x6) diffusion matrix: (Dtt Dtr)
                                      (Drt Drr)

6.965E-07 8.498E-09 -5.937E-09   2.726E-03 -5.020E-04 -1.528E-02
8.505E-09 6.413E-07 3.037E-09   -5.500E-04 8.201E-03 3.784E-03
-5.942E-09 3.048E-09 6.946E-07   -1.534E-02 3.796E-03 -1.295E-02

2.726E-03 -5.500E-04 -1.534E-02   3.833E+06 2.913E+04 -1.685E+05
-5.020E-04 8.201E-03 3.796E-03   2.918E+04 2.889E+06 -3.779E+04
-1.528E-02 3.784E-03 -1.295E-02   -1.686E+05 -3.788E+04 3.748E+06

ROTATIONAL DIFFUSION TENSOR
3.833E+06 2.913E+04-1.685E+05
2.918E+04 2.889E+06-3.779E+04
1.686E+05-3.788E+04 3.748E+06

Anisotropic rotational diffusion
    Eigenvalue (s^-1)   -- Eigenvector ------------
1   2.887E+06   -0.0238 0.9989 0.0392
2   3.617E+06   0.6163 -0.0162 0.7874

3   3.967E+06   0.7872 0.0429 -0.6152

Anisotropic rotational diffusion

    Dx,Dy,Dz (s^-1)   -- Eigenvector ------------

Dz   2.887E+06   -0.0238 0.9989 0.0392

Dy   3.617E+06   0.6163 -0.0162 0.7874

Dx   3.967E+06   0.7872 0.0429 -0.6152

Rotational diffusion coefficient: 3.490E+06 s-1

Rotational diffusion anisotropy: 9.542E+05 s-1

Relaxation time (1): 5.254E-08 s

Relaxation time (2): 5.227E-08 s

Relaxation time (3): 4.690E-08 s

Relaxation time (4): 4.470E-08 s

Relaxation time (5): 4.376E-08 s

Harm. mean relax. (correlation) time: 4.775E-08 s

10. More examples of relaxation decays and NMRD profiles for additional metabolites

Here, we show a set of relaxation decays and relaxation dispersion curves for several metabolites (Fig. S11). In particular, a clear dispersion is observed for isoleucine (Fig. S11d). Weaker dispersions are seen for methanol (Fig. S11e) and valine (Fig. S11g). The error bars for the relaxation decays were derived from experimental noise by considering a region of the spectrum with no visible signal where the standard deviation of the intensity was computed. This value was multiplied by the square root of the number of points in the integrated areas to estimate the confidence intervals for integrals. In the analysis shown in Fig. S11, the error bars for the NMRD profiles are the square root the covariance of relaxation rates in the covariance matrix obtained from the fitting (note that a Monte Carlo procedure was used to derive these confidence intervals for NMRD profiles shown in Fig. 3 and Fig. 5). Other errors, such as errors potentially introduced by the removal of background signals by local baseline correction, were not included and deviations of the rates from expected trends in NMRD profiles may exceed confidence intervals derived from the noise.
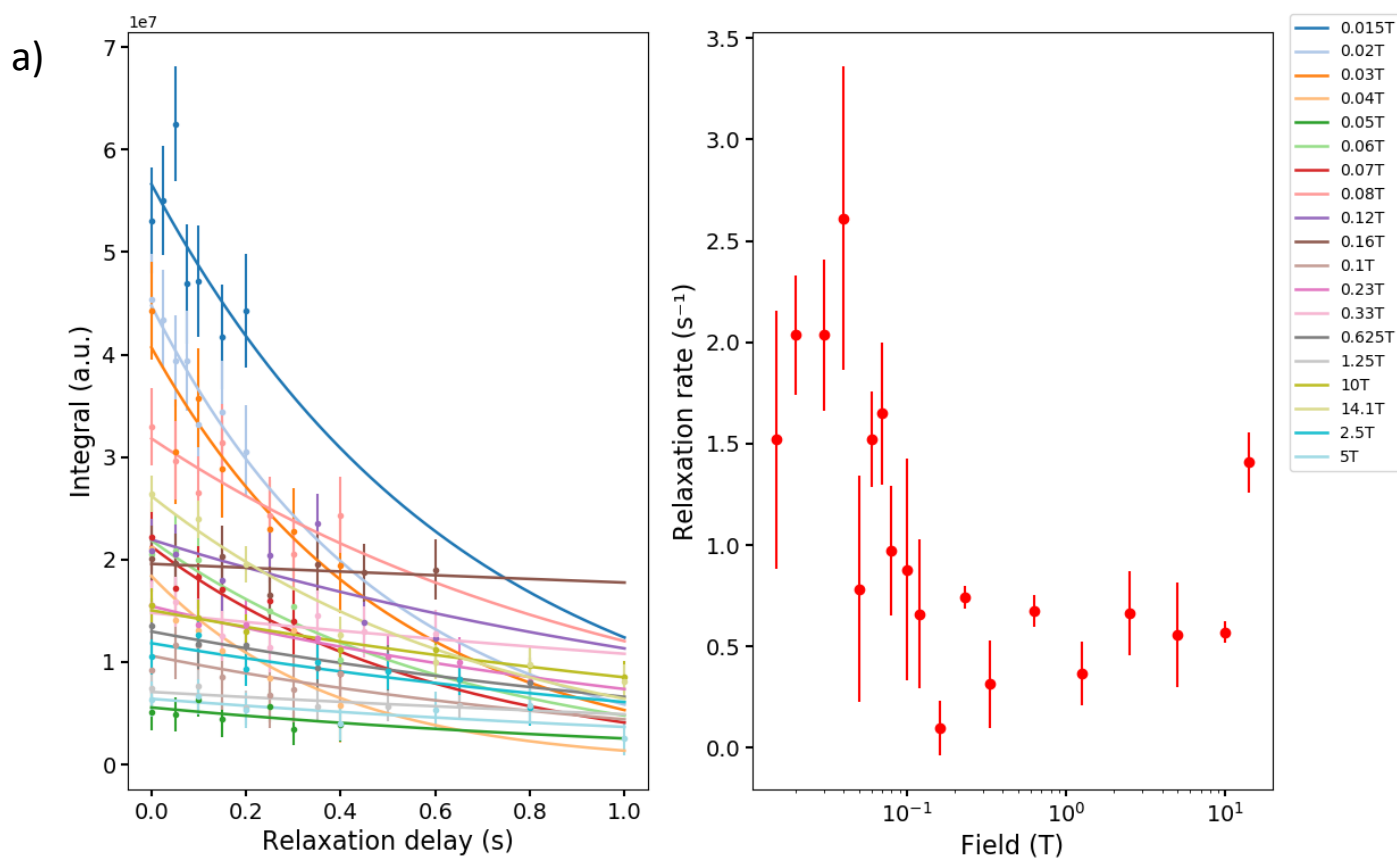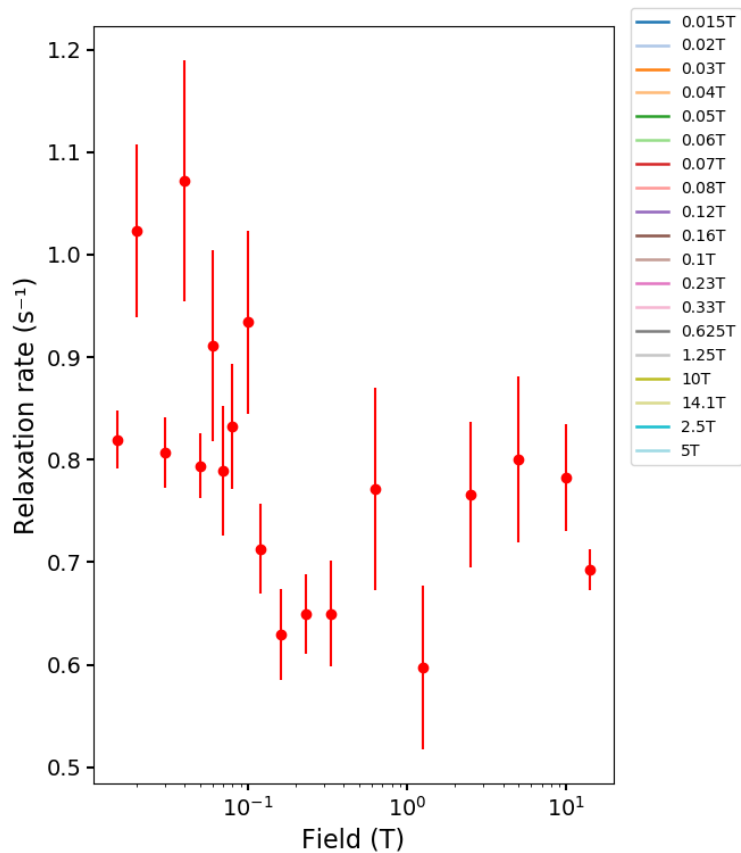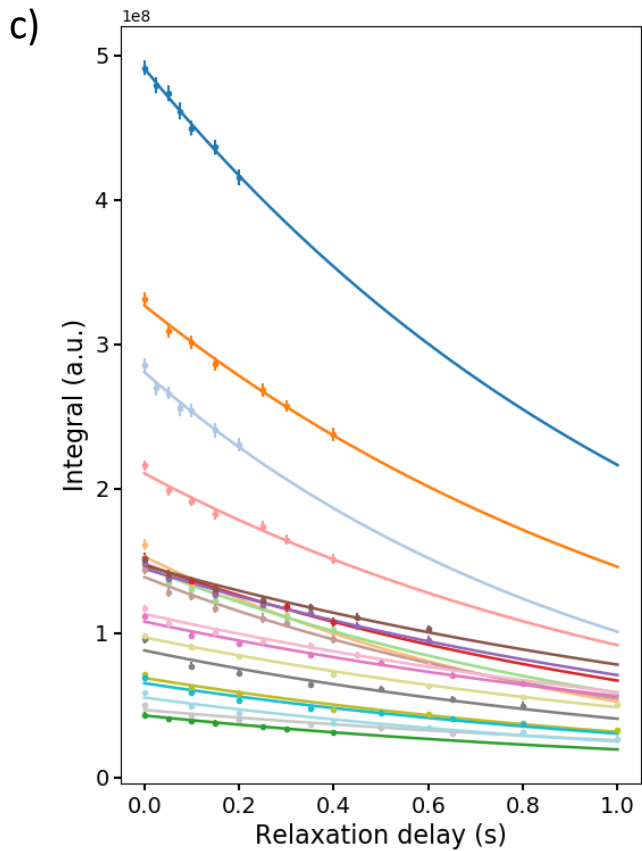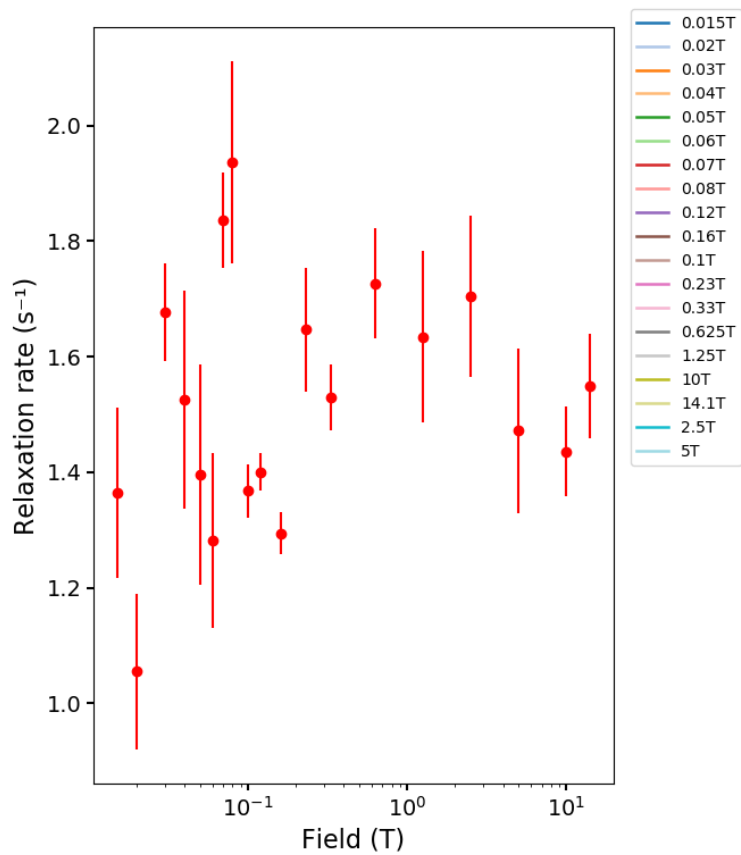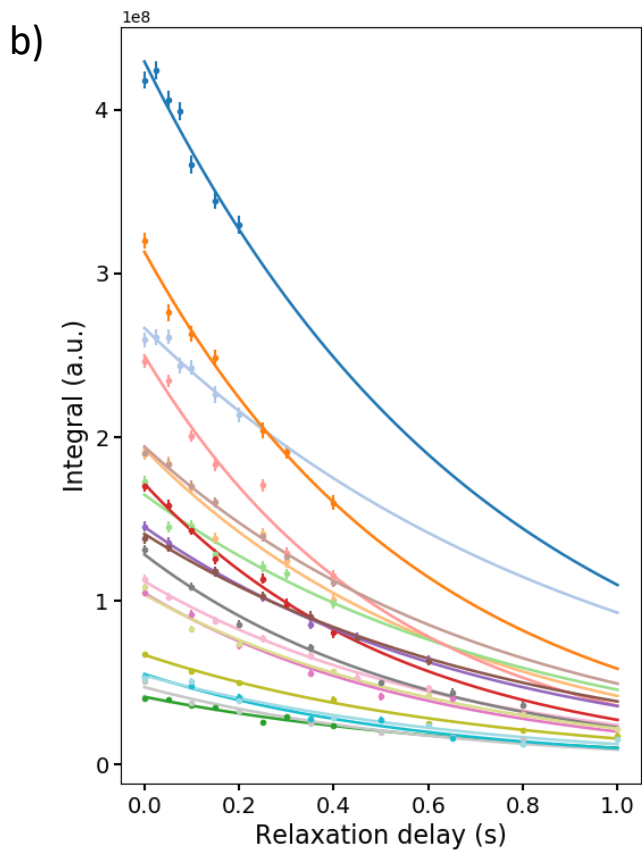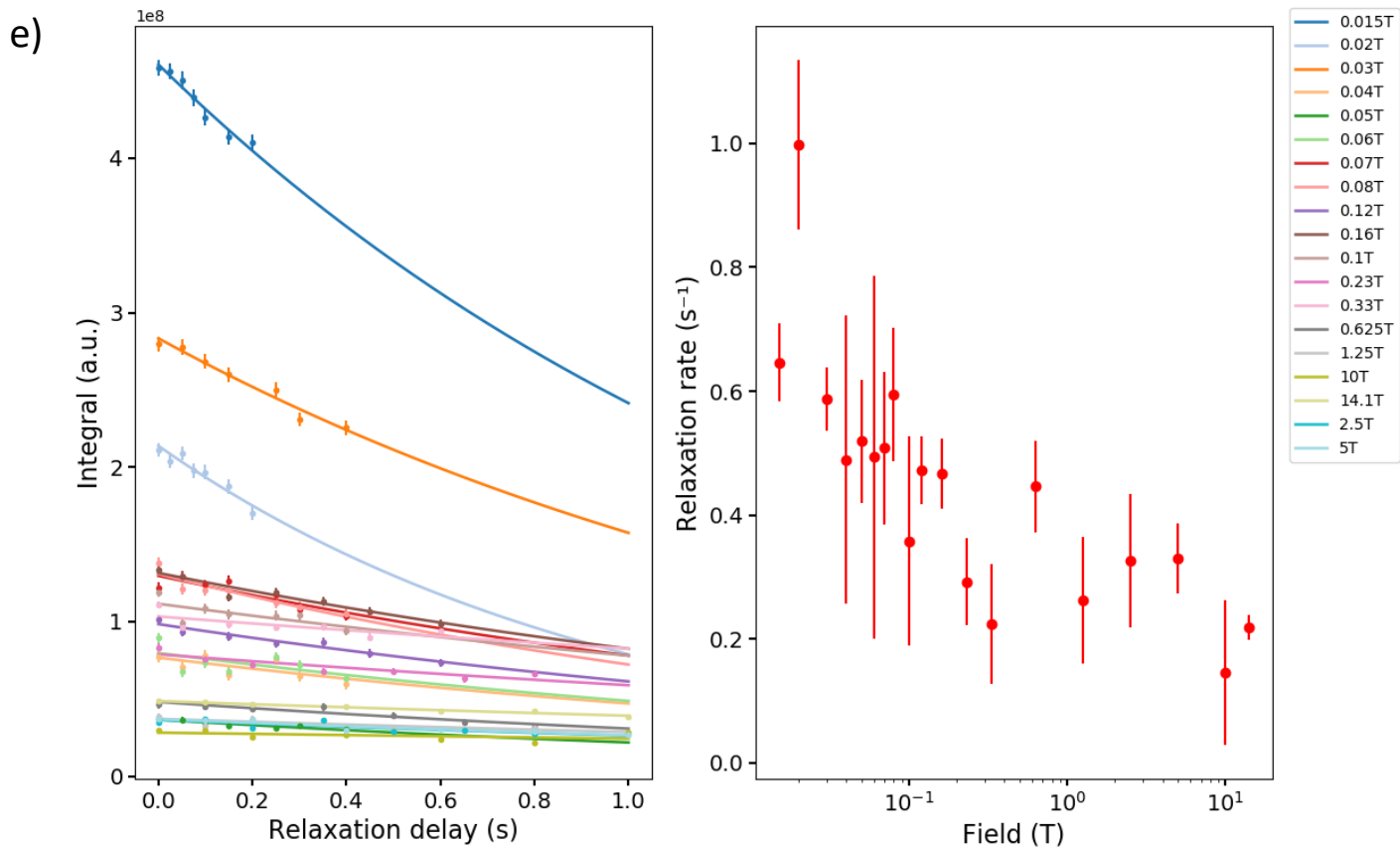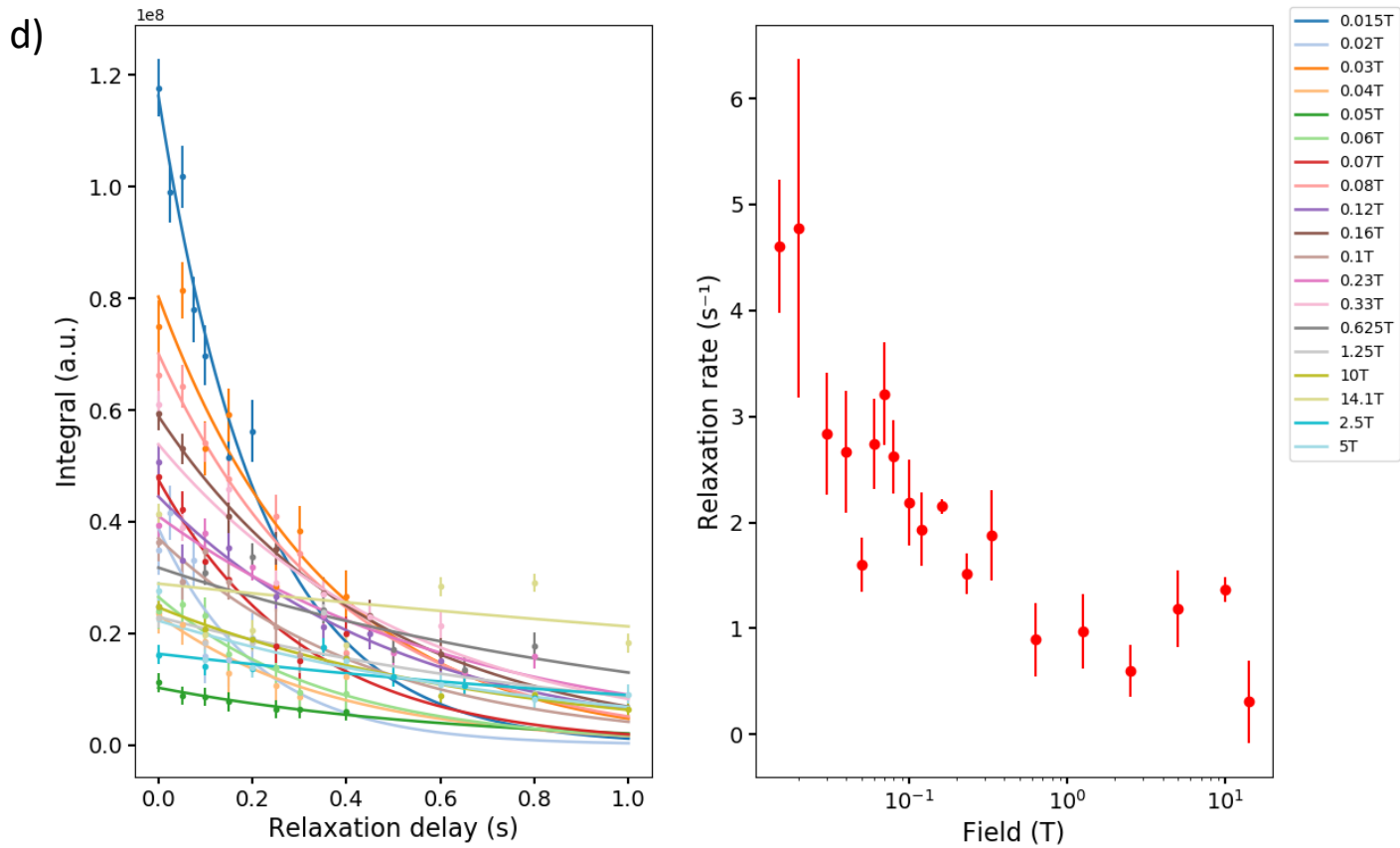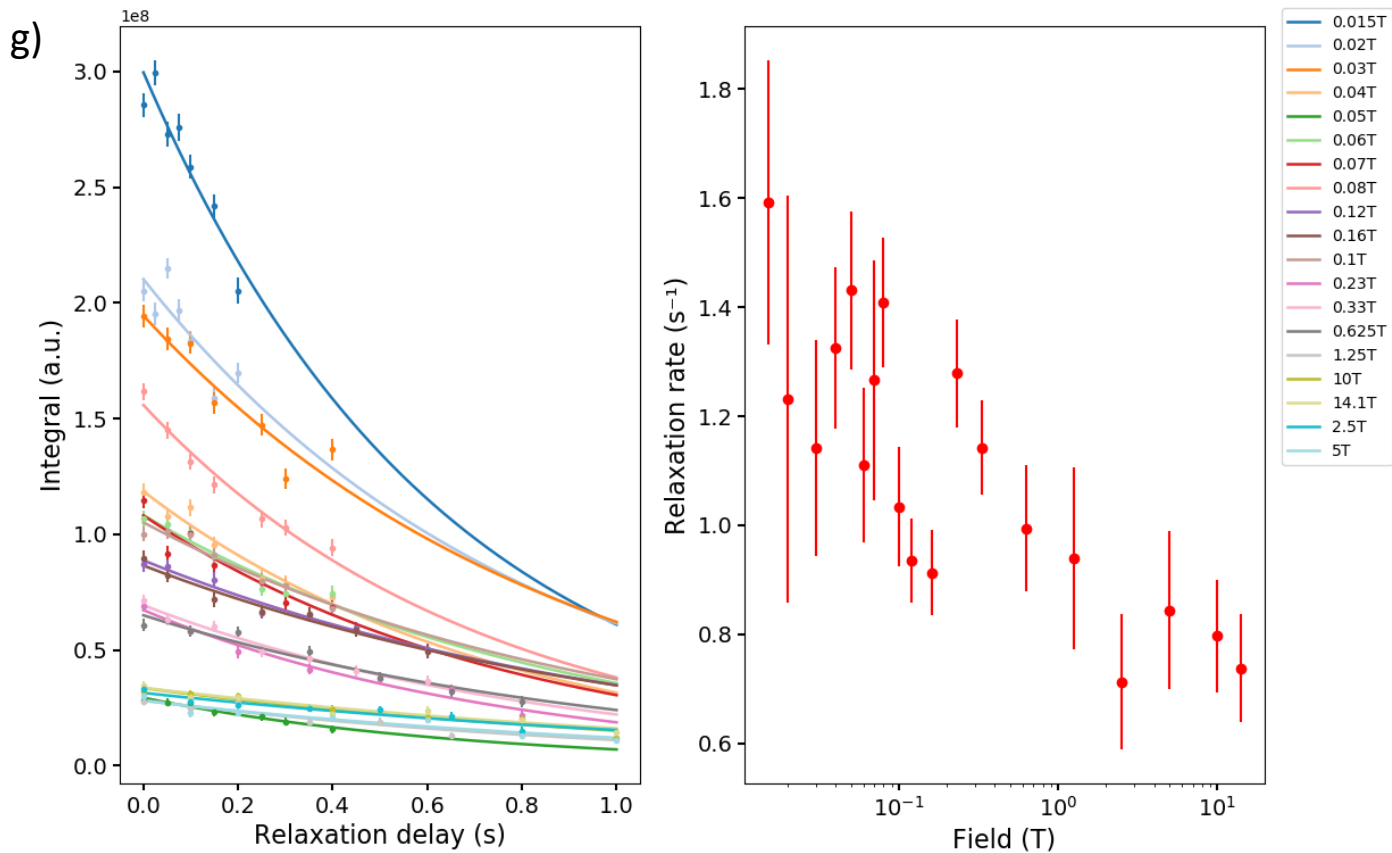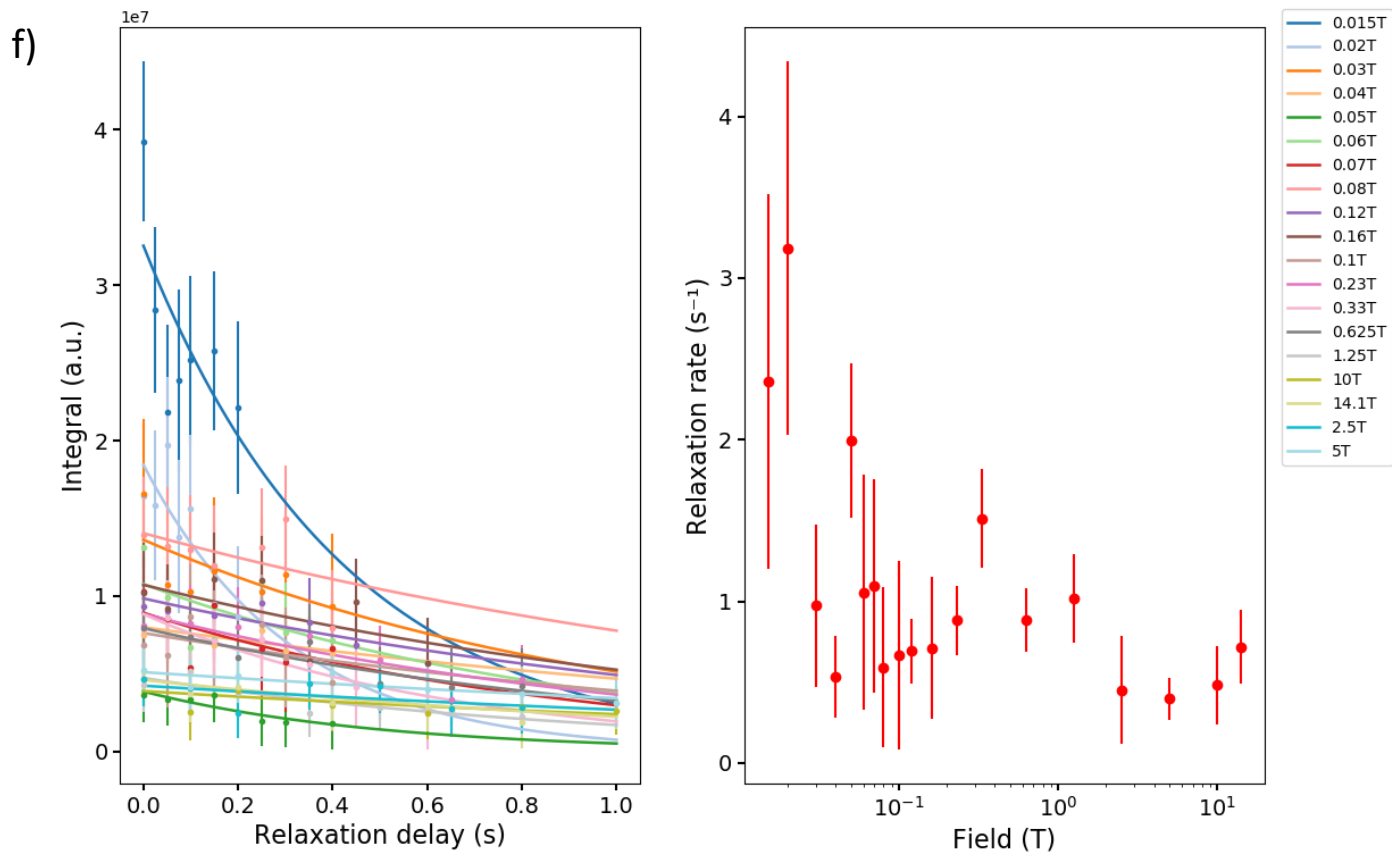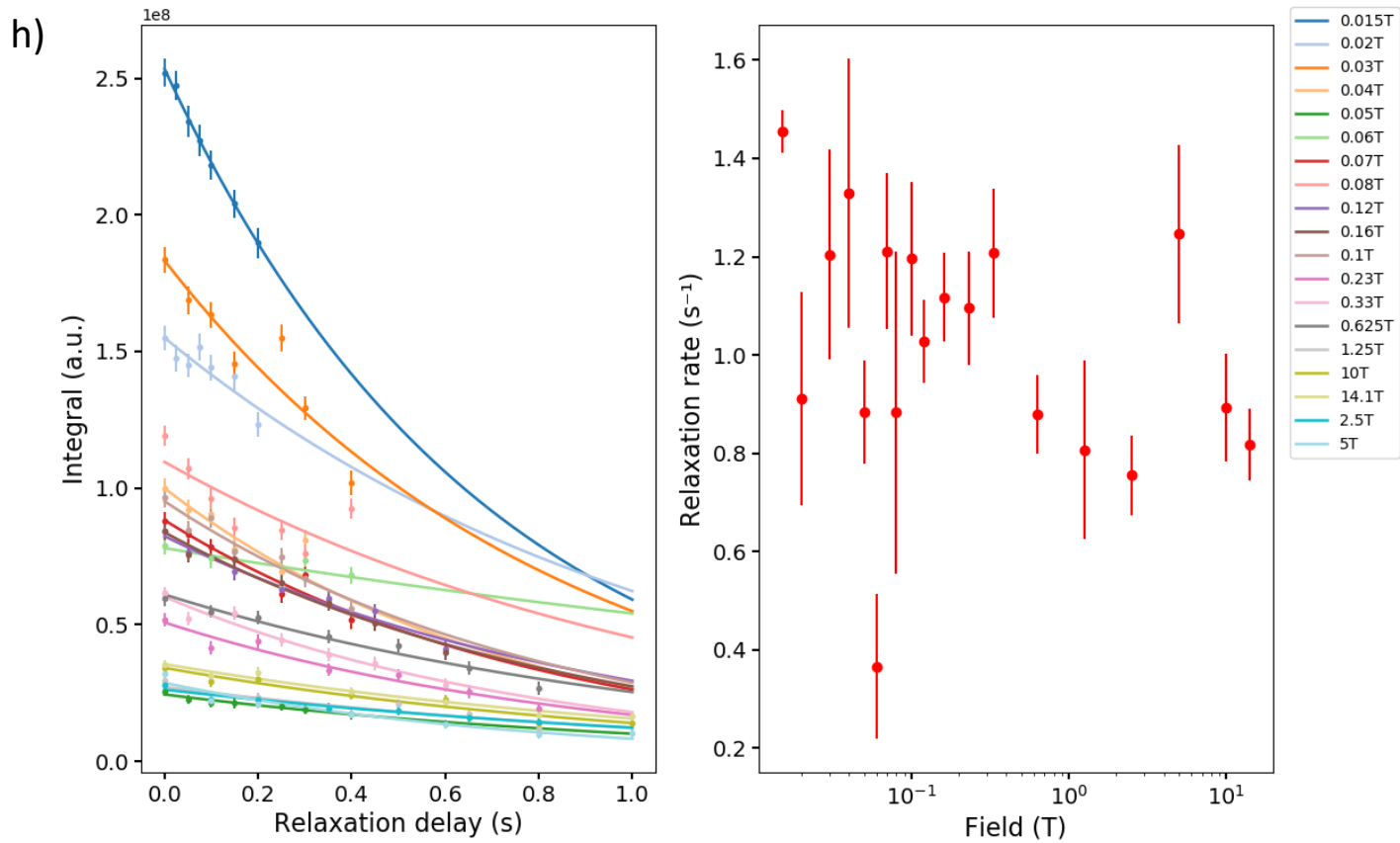
Figure S11. Relaxation decays and NMRD profiles of a) acetone, b) glucose H11, c) glycine, d) isoleucine, e) methanol, f) pyruvate, g) valine H6, h) valine H4.

References

(1)   Beckonert, O.; Keun, H. C.; Ebbels, T. M. D.; Bundy, J.; Holmes, E.; Lindon, J. C.; Nicholson, J. K. *Nature Protocols* **2007**, *2*, 2692.

(2)   Piotto, M.; Saudek, V.; Sklenar, V. *J. Biomol. NMR* **1992**, *2*, 661.

(3)   Akaike, H. *IEEE Transactions on Automatic Control* **1974**, *19*, 716.

(4)   Ortega, A.; Amorós, D.; García de la Torre, J. *Biophys J* **2011**, *101*, 892.

(5)   Tjandra, N.; Feller, S. E.; Pastor, R. W.; Bax, A. *Journal of the American Chemical Society* **1995**, *117*, 12562.

(6)   Woessner, D. E. *The Journal of Chemical Physics* **1962**, *37*, 647.

(7)   Bhagavan, N. V. *Medical biochemistry*; Academic press, 2002.

(8)   Donato, L. J.; Jenkins, S. M.; Smith, C.; Katzmann, J. A.; Snyder, M. R. *American journal of clinical pathology* **2012**, *138*, 398.

(9)   Colombo, S.; Buclin, T.; Decosterd, L. In *7th International Workshop on Clinical Pharmacology of HIV Therapy* 2006, p 20.

(10)   Gordon, S. 2014, p 293.

(11)   Schwaeble, W.; Zwirner, J.; Schulz, T. F.; Linke, R. P.; Dierich, M. P.; Weiss, E. H. *European journal of immunology* **1987**, *17*, 1485.

(12)   Sack, G. H. *Molecular Medicine* **2018**, *24*, 46.

(13)   Takahashi, N.; Ortel, T. L.; Putnam, F. W. *Proceedings of the National Academy of Sciences* **1984**, *81*, 390.

(14)   Wobeto, V. P. d. A.; Zaccariotto, T. R.; Sonati, M. d. F. *Genetics and Molecular Biology* **2008**, *31*, 602.

(15)   De Silva, H. V.; Harmony, J. A. K.; Stuart, W. D.; Gil, C. M.; Robbins, J. *Biochemistry* **1990**, *29*, 5380.

(16)   Refetoff, S. *Endocrine Reviews* **1989**, *10*, 275.

(17)   Pepys, M. B.; Hirschfield, G. M. *The Journal of clinical investigation* **2003**, *111*, 1805.